Department of Physics and Astronomy
University of Heidelberg

Master Thesis in Physics
submitted by

Sophie Elaine Klett

born in Pforzheim (Germany)

2020

Electroweak Symmetry Breaking by Condensates of Fermions in High Color Representations

This Master Thesis has been carried out by Sophie Elaine Klett at the
Max-Planck-Institut für Kernphysik in Heidelberg
under the supervision of
Prof. Dr. Dr. h.c. Manfred Lindner

Abstract

In this thesis we investigate fundamental features of a mechanism that attempts to explain the origin of the electroweak scale by the condensation of fermions in high color representations. Since chiral symmetry in the new fermion sector is dynamically broken due to non-perturbative effects of the running strong coupling this mechanism provides a natural explanation for the scale of the condensate by dimensional transmutation. Electroweak symmetry breaking (EWSB) could then be triggered indirectly via a singlet scalar mediator which couples to the Standard Model Higgs boson and the new fermion sector. In our analysis particular focus is put to the impact of the representation on the condensate and the significance of vector-like fermion masses which explicitly break chiral symmetry. In doing so, we solve the Dyson-Schwinger equation for the fermion propagator within the rainbow-approximation and analyze the behavior of the dynamical mass. In the chiral limit, we find a comparatively larger expectation value (EV) of the condensate for fermions in high representations than for the fundamental representation. A property reflecting the larger Casimir invariants of higher representations. For massive fermions, we propose a method to isolate the non-perturbative contributions to the propagator from the perturbative ones and calculate a lower bound for the EV of the condensate. Our result suggests that in absolute numbers the EV of the condensate increases with mass, while its relative contribution to the dynamical mass diminishes. On the basis of these results, we believe the condensation of a high color fermion with an explicit mass of the order $\sim 10\,\text{TeV}$ could successfully create the scale of EWSB.

Zusammenfassung

In dieser Arbeit untersuchen wir grundlegende Eigenschaften eines Mechanismus zur dynamischen Erzeugung der elektroschwachen Skala durch Kondensation von Fermionen, die unter einer hohen Darstellung der Farbeichgruppe transformieren. Nicht-pertubative Effekte in der laufenden starken Eichkopplung brechen hierbei dynamisch die chirale Symmetrie im Bereich der Fermionen und bieten damit eine natürliche Erklärung für die Entstehung einer neuen Energieskala. Diese Skala kann indirekt, mittels eines neuen Skalars, auf das Standardmodell übertragen werden und so Auslöser der elektroschwachen Symmetriebrechung (ESSB) sein. Bei unserer Analyse steht im Vordergrund welche Auswirkung die Wahl der Repräsentation auf das Kondensat hat und wir gehen der Frage nach, welchen Einfluss ein expliziter Massenterm auf die dynamische chirale Symmetriebrechung hat. Unsere methodische Herangehensweise hierfür ist die Lösung der Dyson-Schwinger Gleichung für den Fermion Propagator innerhalb einer geeigneten Näherung. Im chiralen Grenzfall zeigen unsere Ergebnisse, dass der Erwartungswert des Kondensats für Fermionen in hohen Repräsentationen vergleichsweise größer ist, als für ein Fermion in der fundamentalen Darstellung der Farbeichgruppe. Dies ist eine Eigenschaft, die der größeren Casimir Konstante von hohen Repräsentationen zuzuschreiben ist. Um das Kondensat für ein massives Fermion zu untersuchen, ist es erforderlich die nicht-pertubativen Beiträge zum Propagator von den pertubativen zu trennen. Wir schlagen hierfür ein Verfahren vor mit dem wir in der Lage sind eine untere Grenze für den Erwartungswert des Kondensats anzugeben. Unsere Ergebnisse legen nahe, dass absolut gesehen, der Erwartungswert des Kondensates mit steigender expliziter Masse anwächst, wohingegen der relative Anteil an der gesamten dynamischen Masse abnimmt. Auf Grundlage dieser Ergebnisse nehmen wir an, dass die Skala der ESSB durch das Kondensat eines Fermions mit einer Masse von der Größenordnung $\sim 10\,\text{TeV}$ in einer hohen Darstellung der $SU(3)$ erzeugt werden kann.

Contents

Chapter 1

Introduction

Developments of the past sixty years have led to a successful theoretical description of nature by the Standard Model of particle physics which includes the Glashow-Weinberg-Salam theory of electroweak interactions [1, 2, 3] and the theory of quantum chromodynamics (QCD) [4, 5, 6]. This picture was only recently completed by the discovery of the Higgs boson in 2012 providing an explanation for the generation of fermion and gauge boson masses by the Brout-Englert-Higgs mechanism [7, 8]. Although the Standard Model is a self-consistent theory, we know that it is not a full description of nature as it cannot explain several observations. Among these are neutrino masses, dark matter, matter-antimatter asymmetry or the unification with gravity. In addition, there are some astonishing aspects from theoretical point of view such as the separation of scales.
There emerge three basic energy scales in the Standard Model. These are the Planck scale $M_{\mathrm{pl}} \approx 10^{19}\,\mathrm{GeV}$, where gravity becomes strong, the electroweak scale $v \approx 250\,\mathrm{GeV}$ responsible for the generation of masses and $\Lambda_{\mathrm{QCD}} \approx 200\,\mathrm{MeV}$, where QCD becomes non-perturbative. Ordering from low to high values reveals an inherent hierarchy

$$\Lambda_{\mathrm{QCD}} \lesssim v \ll M_{\mathrm{pl}} \,.$$

The origin of the relatively low value of Λ_{QCD} compared to M_{pl} raises no further questions as this hierarchy of scales finds a natural explanation by the dynamics of the theory. More precisely, the dimensionful scale Λ_{QCD} is created from the logarithmic running of the dimensionless strong coupling, a mechanism commonly known as dimensional transmutation. Nonetheless, we cannot explain the smallness of the electroweak scale by this mechanism. In the first place the large hierarchy between v and M_{pl} constitutes no problem within the Standard Model itself. However with an embedding into a high energy theory naturally the question arises, what stabilizes the electroweak scale against corrections of new physics at high energies. The fundamental issue of this is that there is no symmetry in the Standard Model which protects scalar mass terms from large scale corrections. Usually, the fact that the elctroweak scale is many orders of magnitude smaller than the Planck scale is referred to as the electroweak hierarchy problem.
A possible starting point in attempting to cure this problem is the introduction of classical

scale invariance, which is violated at the quantum level. The electroweak scale can then be generated dynamically by a Coleman-Weinberg mechanism or by dimensional transmutation in a strongly coupled sector.

Imitating the great success of QCD, we will investigate the properties of a model which follows the latter approach. The idea goes back to an initial proposal by Lüst, Papantonopoulos and Zoupanos in 1984 [9, 10]. They suggested to break electroweak symmetry by the condensation of chiral fermions in high color representations, which couple directly to the electroweak sector. An approximation of the gap equation suggest that these condensates generate larger scales than the usual triplet representation as the criticality condition

$$C_2(\mathbf{R})\alpha(\Lambda^2) \gtrsim \mathcal{O}(1) \tag{1.1}$$

is already fulfilled for smaller values of the strong gauge coupling α owing to the larger Casimir constant $C_2(\mathbf{R})$ of a high representation $\mathbf{R}$ [11]. This setting is particularly attractive as it necessitates no new gauge interactions. However nowadays, the original proposal is strongly ruled out by modern measurements of electroweak precision observables such as the well-known Peskin-Takeuchi parameters [12, 13].

This is why we suggest a modified model, where we introduce a vector-like fermion in a high representation of QCD which is a singlet under the remaining Standard Model gauge group. The chiral symmetry breaking condensate of the new fermion can then be used to induce a vacuum expectation value of the Standard Model Higgs boson ϕ by a singlet scalar mediator S

$$\langle\overline{\psi}\psi\rangle \longrightarrow \langle S\rangle \longrightarrow \langle\phi\rangle\,. \tag{1.2}$$

Hence, EWSB is triggered indirectly via the scalar portal. This allows the dynamical generation of scales, although starting from a classically scale invariant scalar sector.

To create a realistic model the high color fermion should have a vector-like explicit mass of at least $\sim \mathcal{O}(1\,\mathrm{TeV})$, in order to escape from current LHC bounds [14]. Even though this introduces a scale to the model, it is technically natural as the fermionic mass term is protected by chiral symmetry.

The main part of this thesis is devoted to the determination of the expectation value of the condensate (or in the following, the condensate for short) for a high color fermion with explicit chiral symmetry breaking mass. Instead of using the approximation of Eq. (1.1), we chose a more thorough method and solve the Dyson-Schwinger equation (DSE) for the fermion propagator in the rainbow-approximation. By this we obtain the dynamical mass which allows us to ascertain properties of the condensate, under usage of the operator product expansion (OPE).

The structure of this thesis will be the following. In chapter 2 we start with an introduction of some general concepts of quantum chromodynamics. Besides an overview over group theoretical aspects, this includes the introduction of the Dyson-Schwinger equation for the fermion propagator within the effective action formalism and a brief review on the OPE technique. Then, in Chapter 3 we explain the approximation scheme within which we solve

the Dyson-Schwinger equation and discuss our numerical strategy. The resulting solutions are presented in Chapter 4. We illustrate the determination of the chiral condensate and subsequently turn to the massive case. Since the solution of the Dyson-Schwinger equation for massive fermions includes both perturbative and non-perturbative contributions, a consistent extraction of the condensate is much more challenging. We approach this difficulty using the OPE and determine a lower bound for the condensate of massive fermions.

Chapter 5 is dedicated to give a brief outlook for the suggested model, especially referring to a possible scale transmission from the new fermion sector to the Standard Model. Finally, in Chapter 6 we recapitulate our results.

Chapter 2

Concepts and Methods of Quantum Chromodynamics

In this chapter we introduce the theoretical framework which will be the footing for the following studies. Starting with the basics of group and representation theory, we will continue to introduce the concept of quantum chromodynamics.
Herein, focus is put on different methods which are commonly used to describe both perturbative and non-perturbative phenomena of the strong interaction.

2.1 Introduction to Group Theory

Symmetry principles belong to the most fundamental tools of physics. Especially in particle physics they play a major role in the construction of quantum field theories, as they are based on local (gauge) symmetries. At the classical level, a symmetry of a field theory can be understood as an invariance of the action with respect to certain transformations of the fields. These transformations can be identified with elements of a group. Thus, symmetries are studied within the mathematical field of group theory.

Generally speaking, a group is a set G of elements together with an operation $\cdot$ such that two elements of the set are mapped to a third one. The set and operation $(G, \cdot)$ must satisfy the following conditions [15]:

- For all $g_1, g_2 \in G$, the operation satisfies $g_1 \cdot g_2 = g_3$ with $g_3 \in G$ (closure) and $(g_1 \cdot g_2) \cdot g_3 = g_1 \cdot (g_2 \cdot g_3)$ (associative),
- there is an identity element $1 \in G$ with $1 \cdot g = g \cdot 1 = g$ for all $g \in G$ and
- for every $g \in G$ there exists a unique inverse element $g^{-1} \in G$, with $g \cdot g^{-1} = g^{-1} g = 1$.

If additionally the group elements commute i. e. $g_1 \cdot g_2 = g_2 \cdot g_1$ for all $g_1, g_2 \in G$, the group is Abelian.

2.1.1 Lie Groups and Lie Algebras

In theoretical particle physics, particular emphasis is put to Lie groups which is a special class of groups with an infinite number of elements, ordered continuously and smoothly [16]. These characteristics make them perfectly suited to describe gauge symmetries and continuous global symmetries. Especially the Lie groups $U(1)$, $SU(2)$ and $SU(3)$ are of importance, as they provide a successful description of the electroweak -and the strong force. Hereafter, we will give a general overview on the basic properties of Lie groups frequently referring to the specific example of $SU(N)$.

An element of a compact Lie group can be represented by the Hermitian group generators T^i , $i = 1, ..., n$ via

$$U(\vec{\alpha}) = \exp\left(-i\sum_{i=1}^{n}\alpha^i T^i\right) \equiv \exp\Big(-i\alpha^i T^i\Big)\,, \tag{2.1}$$

with n continuous parameters α^i that label the group elements [15]. The generators fulfill the commutation relation

$$[T^i, T^j] = if^{ijk}T^k\,, \tag{2.2}$$

where f^{ijk} denotes the structure constant of the group which is totally antisymmetric under index exchange. Together with the commutation relation (2.2), the generators form the according Lie algebra associated to a Lie group. The underlying vector space of the algebra can be identified with the tangent space of the Lie group at the identity [16]. This is why it is possible to describe elements of the group near the identity element (infinitesimal transformations) by the corresponding algebra.
Up to now, the generators T^i are simply abstract operators. If a specific set of $d \times d$ dimensional matrices $T^i_{\mathbf{R}}$ with $i = 1, ..n$ fulfills the commutation relation in Eq. (2.2), this is called a d dimensional representation of the algebra [16]. In analogue, a representation for an element of the group is given by the explicit expression $U(\vec{\alpha}) = \exp(-i\alpha^i T^i_{\mathbf{R}})$.
Throughout this thesis we use the normalization convention

$$\mathrm{Tr}[T^i_{\mathbf{R}}T^j_{\mathbf{R}}] = T(\mathbf{R})\delta^{ij}\,, \tag{2.3}$$

where $T(\mathbf{R})$ is the Dynkin index. A real number that characterizes a representation.
Furthermore, two d dimensional representations $T^i_{\mathbf{R}}$ and $T'^i_{\mathbf{R}}$ are equivalent if there exists a unitary $d \times d$ dimensional matrix O (common for all generators) which relates the two representations by $T'^i_{\mathbf{R}} = O\,T^i_{\mathbf{R}}\,O^\dagger$.
If under such a transformation all generators can simultaneously be block diagonalized, the representation is named reducible. If this is not the case, it is an irreducible representation. The latter play an important role within the Standard Model, since particles transform under irreducible representations of the gauge group.

The above definition yields that reducible representations can be decomposed into irreducible ones under a unitary transformation [17]

$$T^i_{\mathbf{reducible}} \rightarrow \; O\, T^i_{\mathbf{reducible}}\, O^\dagger = \left[\begin{array}{c|c|c} T^i_{\mathbf{irrep_1}} & 0 & \ddots \\ \hline 0 & T^i_{\mathbf{irrep_2}} & \ddots \\ \hline \ddots & \ddots & \ddots \end{array}\right] . \tag{2.4}$$

This process is called Clebsch-Gordan decomposition and we will make use of this property at a later point, when we consider tensor products of representations [15].
Finally, within this context it is useful to define the rank of a Lie group as the number of generators which are simultaneously diagonalizable. In case of the group $SU(N)$, the rank is given by $N-1$.

2.1.2 Casimir Invariants

In general, Casimir invariants are sets of operators which commute with all generators of the group. Therefore, the number of Casimir operators corresponds to the rank of the group and their eigenvalues are suitable to label irreducible representations [1].
The group $SU(N)$ has $N-1$ Casimir operators. Conclusively, an irreducible representation can be described by $N-1$ quantum numbers [18].
In the subsequent, we are especially interested in the characteristics of the quadratic Casimir operator that is defined by

$$C_2(\mathbf{R})\mathbb{1} = \sum_{i=1}^{n} T^i_{\mathbf{R}} T^i_{\mathbf{R}}\,, \tag{2.5}$$

a quantity being proportional to the identity matrix by Schur's lemma [17].
The quadratic Casimir operator and the Dynkin index of a representation are related by [16]

$$T(\mathbf{R})\, n = C_2(\mathbf{R}) d(\mathbf{R})\,, \tag{2.6}$$

where n is the number of generators of the group and $d(\mathbf{R})$ is the dimension of the representation. For $SU(N)$, the number of generators is given by N^2-1.
At this point we remark that for every representation $\mathbf{R}$ there exits a complex conjugate representation $\overline{\mathbf{R}}$, whose generators are given by

$$T^i_{\overline{\mathbf{R}}} = -\left(T^i_{\mathbf{R}}\right)^* . \tag{2.7}$$

[1] This concept is also applied for spin and angular momentum, where the Casimir operator $\vec{J}^2 = \sum_i J^i J^i$ commutes with all generators J^i of the underlying SU(2) and its eigenvalue $j(j+1)$ labels an irreducible representation.

In the next section it will be evident that there is need for such conjugate representations in order to describe adjoint fields (see Sec. 2.2).
With regard to the different representations of a Lie Algebra we highlight the two most common ones. This is the fundamental or defining representation and the adjoint representation [16]. The former is the smallest representation which is non-trivial. For $SU(N)$, generators in the fundamental representation are given by N^2-1 Hermitian and traceless matrices of dimension $N \times N$.
Contrary, the adjoint representation acts on the vector space which is spanned by the generators themselves. Hence, in case of $SU(N)$ with N^2-1 generators, it is a N^2-1 dimensional representation which can be defined via the structure constants according to [17]

$$(T^i_{\text{adj}})^{jk} = -if^{ijk}\,. \tag{2.8}$$

Within the standard model these two representations play a major role, since fermions which are charged under some $SU(N)$ gauge group, transform according to the fundamental representation, while the corresponding gauge bosons transform in the adjoint representation.
To give an explicit example we consider the group $SU(2)$. In the fundamental representation the three generators of the group are proportional to the Pauli matrices $\vec{\sigma} = (\sigma^1, \sigma^2, \sigma^3)$. Typically, one uses the normalization convention $T^i_{\text{fund}} \equiv \sigma^i/2$ so that the Dynkin index for the fundamental representation is $1/2$. From the commutation relation of the Pauli matrices one can deduce that the structure constants are given by the Levi-Civita tensor $f^{ijk} = \epsilon^{ijk}$. Therefore, the adjoint representation is provided by the three 3×3 dimensional matrices whose entries can be written like $(T^i_{\text{adj}})^{jk} = -i\epsilon^{ijk}$.
As a second example, attention is put to the group $SU(3)$. Its defining representation is usually provided by the eight 3×3 Gell-Mann matrices λ^i through $T^i_{\text{fund}} = \lambda^i/2$ (see Appendix A.3) from which the structure constants can be calculated. The Gell-Mann matrices are traceless and two of them (conventionally λ^3 and λ^8) are simultaneously diagonalizable. Thus, the group has rank two.

2.1.3 Representations of $SU(3)$

The aforementioned representations play an important role within the Standard Model. However for this study, we are especially interested in exotic irreducible representations of the color gauge group. Their characterization in terms of the quadratic Casimir constant and Dynkin index is of particular importance for our investigation. Therefore, we calculate these specific quantities for the ten lowest dimensional representations in the subsequent. We will use the common convention to label representations by their dimension. The existence of two representations with same dimension but different Casimir constant will be indicated by a prime.
Since the group $SU(3)$ has rank two, an irreducible representation can be described by two quantum numbers (p, q) with $p, q = 0, 1, 2, \ldots$.

Not going into mathematical details of a derivation, the dimension of a $SU(3)$ representation can then be calculated using [18]

$$d(\mathbf{R}) = \frac{1}{2}(p+1)(q+1)(p+q+2)\,, \tag{2.9}$$

and the quadratic Casimir constant is given by [19]

$$C_2(\mathbf{R}) = \frac{1}{3}\left(p^2 + q^3 + 3p + 3q + pq\right)\,. \tag{2.10}$$

Together with the relationship in Eq. (2.6), one can calculate the Dynkin index. For the lowest dimensional irreducible representations the resulting values are listed in Tab. 2.1. For a representation $\mathbf{R}$ with quantum numbers (p, q), the complex conjugated representation $\overline{\mathbf{R}}$ is characterized by (q, p). The formula in Eq. (2.10) yields that the Casimir constant is symmetrical under the exchange $p \leftrightarrow q$ and therefore $C_2(\mathbf{R}) = C_2(\overline{\mathbf{R}})$. Analogously this also applies to the Dynkin index.

Rep (R)	(p, q)	$\mathbf{C_2(R)}$	$T(R)$
1	(0, 0)	0	0
3	(1, 0)	4/3	1/2
6	(2, 0)	10/3	5/2
8	(1, 1)	3	3
10	(3, 0)	6	15/2
15	(2, 1)	16/3	10
15'	(4, 0)	28/3	35/2
21	(0, 5)	40/3	35
24	(1, 3)	25/3	25
27	(2, 2)	8	27

Table 2.1 List of lowest dimensional $SU(3)$ representations with their according Casimir constant and Dynkin index, following the conventions from [20].

2.2 Introduction to Quantum Chromodynamics

The theory of strong interaction is described by QCD which bases on the color gauge group $SU(N_c)$ with $N_c = 3$ [16]. Fermions that carry color charge experience the strong force and interact with the gauge bosons, called gluons. In the Standard Model, there are $n_F = 6$ different flavors of strongly interacting spin-1/2 particles that are named quarks. They transform in the fundamental representation $\mathbf{R} = \mathbf{3}$, while their anti-particles transform in the anti-fundamental representation $\mathbf{R} = \overline{\mathbf{3}}$. Hence, the quark fields can be seen as three component vectors in color space. Contrary, the gauge bosons transform in the adjoint representation $\mathbf{R} = \mathbf{8}$. Thus, there are eight gluon fields A^i, i = 1, ..., 8.
In the subsequent, we elaborate how the interaction between quarks and gluons is described

within the Standard Model. Nevertheless, we emphasize that the following concepts can also be applied to fermions in general representations.

2.2.1 QCD Lagrangian

As in other field theories, the interaction between gauge bosons and fermions is described by a Lagrangian which is invariant under local gauge transformations [21]. For QCD the Lagrangian is given by [2]

$$\mathcal{L}_{\mathrm{QCD}} = \sum_{f=1}^{n_F} \overline{\psi_f} \left(i \not{D} - m_{0f} \right) \psi_f - \frac{1}{4} F^i_{\mu\nu} F_i^{\mu\nu} \,. \tag{2.11}$$

In our notation ψ_f is the Dirac spinor, which represents the quark field of flavor f, and $\overline{\psi_f} \equiv \psi_f^\dagger \gamma_0$ is the Dirac adjoint. Together, this spinor structure guarantees Lorentz invariance of the first part of the Lagrangian. We note that for simplicity the Dirac indices of the quark spinors as well as the quark color indices are omitted. The current quark mass m_{0f} is actually generated by spontaneous symmetry breaking in the full Standard Model [7, 8]. Nonetheless, considering QCD alone it can be seen as an explicit mass term. The gauge covariant derivative is defined as

$$D^\mu = \partial^\mu + i g_0 T^i A_i^\mu \,, \tag{2.12}$$

where the T^i are the generators of $SU(3)$ and g_0 is the strong coupling constant.
The dynamics of the gluon field are described by the last term of the Lagrangian, where the field strength tensor of the gluon field is given by

$$F_i^{\mu\nu} = \partial^\mu A_i^\nu - \partial^\nu A_i^\mu - g_0 f_{ijk} A^{\mu\, i} A^{\nu\, k} \,, \tag{2.13}$$

with the structure constant f_{ijk} defined in Eq. (2.2). In a short hand notation, we can write $A^\mu \equiv A_i^\mu T^i$ and equivalently $F^{\mu\nu} \equiv F_i^{\mu\nu} T^i$, where the sum over index i is implicit. Considering the trace identities that are satisfied by the $SU(3)$ generators (see Appendix A.3) the last term of the Lagrangian can be rewritten by

$$\frac{1}{4} F^i_{\mu\nu} F_i^{\mu\nu} = \frac{1}{2} \mathrm{Tr}[F_{\mu\nu} F^{\mu\nu}] \,. \tag{2.14}$$

Together, the covariant derivative and the field strength tensor fulfill the commutation relation $-(i/g_0)[D^\mu, D^\nu] = F^{\mu\nu}$.

[2] The QCD Lagrangian in principle contains a further term allowed by gauge symmetry and renormalizability that is $\sim \theta_{QCD} F^i_{\mu\nu} \tilde{F}_i^{\mu\nu}$. Here, $\tilde{F}_i^{\mu\nu} \equiv (1/2)\epsilon_{\mu\nu\rho\sigma} F_i^{\rho\sigma}$ denotes the dual field strength tensor. Contrary to the other terms in Eq. (2.11), it violates P (parity), T (time reversal) and CP (charge-parity) symmetry for $\theta_{QCD} \neq 0$ which is also referred to as the strong CP problem. Nevertheless, since this term has no impact on the following discussion, we will neglect in the succeeding [16].

2.2.2 Gauge Invariance and Gauge Fixing

The requirement for all terms of the Lagrangian in Eq. (2.11) is to be gauge invariant under $SU(3)$ transformations. Therefore, we will investigate how the different fields transform in order to demonstrate that gauge invariance is fulfilled.

Under a gauge transformation, the fermion field transforms as

$$\psi(x) \longrightarrow \psi'(x) = U(x)\psi(x) \ , \tag{2.15}$$

where $U(x) \in SU(3)$ is a local, unitary transformation that is given by $U(x) = \exp\Big(-ig_0\alpha_i(x)T^i\Big)$ and the $\alpha_i(x)$ denote space-time dependent functions that characterize the transformation. Then, following from the definition of the adjoint fermion field, $\overline{\psi}(x)$ transforms as

$$\overline{\psi}(x) \longrightarrow \overline{\psi}'(x) = \overline{\psi}(x)U^\dagger(x) \ . \tag{2.16}$$

Since $U(x)$ is unitary, the explicit mass term for fermions is evidently invariant under $SU(3)$ transformations.
Considering that part of the Lagrangian which includes the covariant derivative, gauge invariance is not instantly obvious. This is due to the fact that the derivative also acts on the local transformation $U(x)$ itself. Though, with the gluon field transforming according to

$$A^\mu(x) \longrightarrow A^{\mu\prime}(x) = U(x)\left(A^\mu(x) - \frac{i}{g_0}\partial^\mu\right)U^{-1}(x)\,, \tag{2.17}$$

it can be shown that the covariant derivative fulfills the transformation rule

$$D_\mu\psi(x) \longrightarrow D'_\mu\psi'(x) = U(x)(D_\mu\psi(x))\,, \tag{2.18}$$

Thus, the term $\overline{\psi}(x)\not{D}\psi(x)$ is gauge invariant as well. With regard to the definition of the field strength tensor, Eq. (2.17) yields the transformation property

$$F^{\mu\nu}(x) \longrightarrow F^{\mu\nu\prime}(x) = U(x)F^{\mu\nu}(x)U^{-1}(x)\,. \tag{2.19}$$

Hence, following from the cyclicity of the trace operator, Eq. (2.14) is invariant and therefore the complete Lagrangian of QCD exhibits invariance under gauge transformations.

Proceeding from that, we define the action

$$S_{\mathrm{QCD}}(A,\overline{\psi},\psi) = \int d^4x\mathcal{L}_{\mathrm{QCD}}\,. \tag{2.20}$$

By construction, the action is invariant along the gauge orbit, which is the set of all possible gauge transformations of a given field configuration $\mathcal{O}(A,\overline{\psi},\psi) = \{(A',\overline{\psi'},\psi')|U(x) \in$

$SU(3)\}$. In the path integral formalism, the gauge theory is defined by the generating functional [21]

$$\mathcal{Z}(j,\overline{\eta},\eta,\overline{\sigma},\sigma) = \int \mathcal{D}[A,\overline{\psi},\psi,\overline{c},c] \exp\left(-S_{\mathrm{QCD}}(A,\overline{\psi},\psi) - S_{GF}(A,\overline{c},c) + S_C\right), \quad (2.21)$$

where S_C is the source term that contains the local sources $j,\overline{\eta},\eta,\overline{\sigma}$ and σ

$$S_C = \int d^4x \left[A_i^\mu j_\mu^i + \overline{\eta}\psi + \overline{\psi}\eta + \overline{\sigma}c + \overline{c}\sigma\right]. \quad (2.22)$$

To avoid the integration over physically equivalent field configurations within one gauge orbit, the gauge fixing term

$$S_{GF}(A,\overline{c},c) = \int d^4x \left[-\frac{(\partial_\mu A_i^\mu)^2}{2\xi} + (\partial_\mu \overline{c}^{\,i})(D_{ij}^\mu c^j)\right] \quad (2.23)$$

is added to classical action [22]. This introduces unphysical auxiliary fields $\overline{c}^{\,i}$ and $c^{\,i}$ that are anti-commuting spin-0 fields, named ghosts. The covariant derivative in the adjoint representation is given by $D_{ij}^\mu = \delta_{ij}\partial^\mu + g_0 f_{ijk} A^{\mu\,k}$ and ξ denotes the gauge parameter which in principle can be selected freely.
There are two widely spread choices for ξ. These are first of all Feynman gauge where $\xi \to 1$ and secondly, Landau gauge with $\xi \to 0$. In the following we will use the latter, since the calculations of the next sections will be more simple [11]. The according gauge condition for Landau gauge is given by $\partial_\mu A_i^\mu = 0$. Hence, gluon fields are purely transverse.
Putting all together, the gauge fixed QCD Lagrangian reads

$$\mathcal{L}_{\mathrm{full}} = \mathcal{L}_{\mathrm{QCD}} - \frac{(\partial_\mu A_i^\mu)^2}{2\xi} + (\partial_\mu \overline{c}^{\,i})(D_{ij}^\mu c^j). \quad (2.24)$$

Evidently, it does no longer possess local gauge invariance, but it has a BRST symmetry [23, 24] which ensures that physical observables are independent of the gauge.

2.2.3 Phenomenological Aspects

Before we proceed, we want to mention several interesting aspects that characterize the strong interaction. As we have outlined, QCD bases on the non-Abelian gauge group $SU(3)$ and is therefore usually called a non-Abelian gauge theory. A consequence of this property is that the vacuum polarization of the gluon propagator does not only receive contributions by fermion loops but also by gauge boson self-interactions and interactions with ghosts (see Fig. 2.1). The absorption of these vacuum polarization diagrams into the coupling constant leads to an effective running coupling that depends on the considered momentum scale [25]. As a result, the various contributions have a different impact on the effective coupling [26]. Simply speaking, the contributions of the fermion loop have a screening effect on the color charge at long distances that makes the effective force weaker. Contrary, the gluon loops

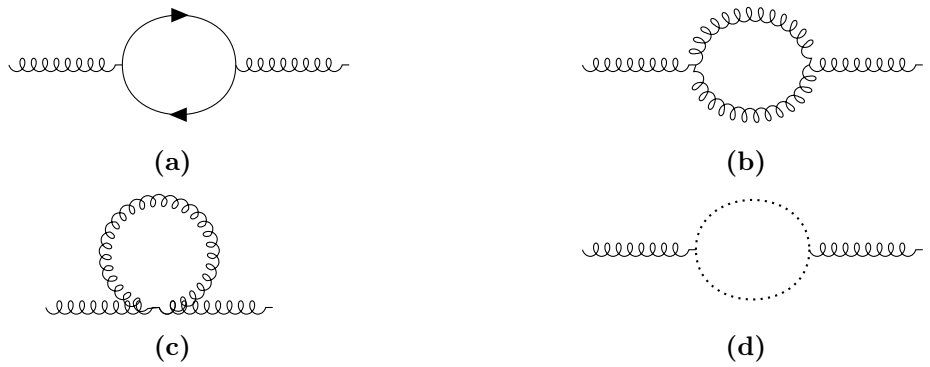

Figure 2.1 Feynman graphs that contribute at one-loop to the gauge boson self-energy in QCD by a fermion loop a), gauge boson loop b), c) and ghost loop d).

have an anti-screening character. Therefore, the basic behavior of the running coupling depends on the number as well as on the representation of the fermions that participate in the strong interaction. We will elaborate details on this in Sec. 2.6.1 . For now we note that within the Standard Model the anti-screening effect of the gluons is dominant. Therefore, the strong force becomes weak at high momentum (asymptotic freedom) and grows strong at low momentum (confinement) [11]. This leads to a complete different phenomenology then in Abelian theories such as quantum electrodynamics (QED), where only the first diagram in Fig. 2.1 contributes to the one-loop vacuum polarization of the gauge boson.
The non-perturbative growing of the strong coupling constant sets a characteristic energy scale $\Lambda_{\mathrm{QCD}} \sim 200$ MeV [27] where the coupling becomes non-perturbative. This mechanism is also called dimensional transmutation, since the scale is dynamically generated from the (logarithmic) running of a dimensionless coupling.
We will focus now on the symmetry aspects. Ignoring the bare quark masses, the QCD Lagrangian is not only invariant under the gauge group but exhibits a further symmetry, namely a global chiral flavor symmetry $U(n_F)_L \times U(n_F)_R$ [3]. Since in the Standard Model the quarks have non-zero masses, this global symmetry is broken. In particular, the masses of the four heaviest quarks break this symmetry badly, while the two lightest quarks can be considered as almost massless. This is why we can resort to the useful approximate $U(2)_L \times U(2)_R$ symmetry, which can be further decomposed into a product of groups, so that the continuous symmetries of $\mathcal{L}_{\mathrm{QCD}}$ are given by

$$\underbrace{SU(3)_C}_{\text{gauge}} \times \underbrace{SU(2)_L \times SU(2)_R \times U(1)_B \times U(1)_A}_{\text{global}} . \tag{2.25}$$

In the above, the two $U(1)$ factors represent Baryon number and axial Baryon number, respectively [4].
It is now due to the non-perturbative growing of the strong coupling that in QCD at long

[3] The indices L and R denote independent transformations for fields of left -and right-handed chirality.
[4] Baryon number is an accidental symmetry that is conserved by QCD, while the axial Baryon number is broken by non-perturbative effects related to the triangle anomaly [28].

distances, the vacuum rearranges and a condensate forms which is a non-zero vacuum expectation value (VEV) of the composite operator

$$\langle \overline{\psi}\psi \rangle \neq 0 \,. \tag{2.26}$$

Decomposing the Dirac fields into left -and right handed Weyl fields by the usual projection operators $\psi_L = P_L\psi$ and $\psi_R = P_R\psi$ reveals that the condensate decomposes as

$$\langle \overline{\psi}\psi \rangle = \langle \overline{\psi_L}\psi_R + \overline{\psi_R}\psi_L \rangle \,. \tag{2.27}$$

Thus, it becomes clear that a non-zero VEV breaks the approximate chiral symmetry. This process is also called dynamical chiral symmetry breaking [29].

2.3 Color Potential

Before going into the details of the dynamics of chiral symmetry breaking, we want to investigate the question what can be said from a purely group theoretical point of view about the color force between two fermions. To raise the discussion on more general grounds, we consider fermions that transform under a general irreducible representation of the color gauge group in the following.
From the Lagrangian in Eq. (2.11) one can deduce the Feynman rule which corresponds to the interaction of a gluon with a fermion in representation $\mathbf{R}$ of $SU(3)$. This is given by

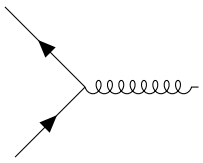

$$\sim \quad g_0 \gamma^\mu T^i_{\mathbf{R}} \,, \tag{2.28}$$

where we indicate the color index i of the gluon as well as the Dirac index μ of the vertex. In the most simple approach to study the force between two fermions in representations $\mathbf{R_1}$ and $\mathbf{R_2}$, we assume that they interact by the exchange of a single gluon. Then, according to the Feynman rule in Eq. (2.28) the diagram that is shown in Fig. 2.2 is proportional to the factor $\sim g_0^2 T^i_{\mathbf{R_1}} T^i_{\mathbf{R_2}}$(where no sum over i is assumed) and the sum over the exchange of all eight possible gluons ultimately leads to a color potential being proportional to

$$V \sim g_0^2 \sum_{i=1}^{8} T^i_{\mathbf{R_1}} T^i_{\mathbf{R_2}} \,. \tag{2.29}$$

Before we evaluate this expression further, it is necessary to take a short look on the tensor product $\mathbf{R_1} \otimes \mathbf{R_2}$ of the two representations. In this way we can consider all possible color combinations of the two initial fermions to a single state.

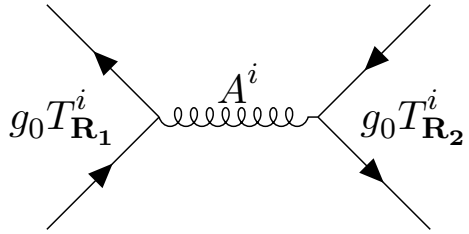

Figure 2.2 Feynman graph which creates the color potential between two fermions in $SU(3)$ representations $\mathbf{R_1}$ and $\mathbf{R_2}$ in the one gluon exchange approximation.

To give an example, the tensor product of a $\mathbf{3}$ and a $\overline{\mathbf{3}}$ representation of $SU(3)$ can be decomposed into the irreducible representations $\mathbf{3} \otimes \overline{\mathbf{3}} = \mathbf{1} \oplus \mathbf{8}$ [20].
From the group theoretical point of view, this means that a quark in fundamental representation and an anti-quark in anti-fundamental representation can combine to an object that either transforms as a singlet (not feeling the strong force anymore) or an 8-plet. Apparently, it is of great importance, which color state is selected. Going back to the general case, the generators of a tensor product are given by the sum of generators of the single representations [30]

$$T^i_{\mathbf{R_1} \otimes \mathbf{R_2}} = T^i_{\mathbf{R_1}} \otimes \mathbb{1}_{\mathbf{R_2}} + \mathbb{1}_{\mathbf{R_1}} \otimes T^i_{\mathbf{R_2}} \,. \tag{2.30}$$

In a short notation we write $T^i_{\mathbf{R_1} \otimes \mathbf{R_2}} = T^i_{\mathbf{R_1}} + T^i_{\mathbf{R_2}}$ in a sense that $T^i_{\mathbf{R_1}}$ only acts on $\mathbf{R_1}$ indices and the same for $\mathbf{R_2}$.
With this knowledge we can evaluate Eq. (2.29) in terms of the Casimir constants of the representations [31]

$$\begin{aligned} \sum_i T^i_{\mathbf{R_1}} T^i_{\mathbf{R_2}} &= \frac{1}{2} \sum_i \left[\left(T^i_{\mathbf{R_1} \otimes \mathbf{R_2}} \right)^2 - \left(T^i_{\mathbf{R_1}} \right)^2 - \left(T^i_{\mathbf{R_2}} \right)^2 \right] \\ &= \frac{1}{2} \left[C_2(\mathbf{R_1} \otimes \mathbf{R_2})_c - C_2(\mathbf{R_1}) - C_2(\mathbf{R_2}) \right] , \end{aligned} \tag{2.31}$$

where $C_2(\mathbf{R_1} \otimes \mathbf{R_2})_c$ is the Casimir constant of the irreducible representation that the two fermions are combined to.
To continue with the above example of the fermions being in fundamental and anti-fundamental representation, we can calculate the color potential for the two possible cases that are [25]

- $\overline{\psi}\psi$ form a singlet: $V \sim \left(\frac{1}{2} C_2(\mathbf{1}) - C_2(\mathbf{3}) - C_2(\overline{\mathbf{3}}) \right) = -\frac{4}{3}$,
- $\overline{\psi}\psi$ form an 8-plet: $V \sim \left(\frac{1}{2} C_2(\mathbf{8}) - C_2(\mathbf{3}) - C_2(\overline{\mathbf{3}}) \right) = +\frac{1}{6}$.

The chosen conventions are such that a minus sign indicates an attractive potential. Therefore, a quark and an anti-quark can form an uncolored bound state (singlet). Meanwhile, there cannot be a bound 8-plet state, due to the repulsive nature of the color potential.

$\mathbf{R_1}$	$\mathbf{R_2}$	$(\mathbf{R_1} \otimes \mathbf{R_2})_c$	$V \propto$
6	$\overline{\mathbf{6}}$	**1**	$-\frac{10}{3}$
6	$\overline{\mathbf{6}}$	**8**	$-\frac{11}{6}$
6	$\overline{\mathbf{6}}$	**27**	$+\frac{4}{3}$
6	**6**	**6**	$-\frac{5}{3}$
6	**6**	**15**	$-\frac{2}{3}$
6	**6**	$\mathbf{15'}$	$+\frac{4}{3}$
6	$\overline{\mathbf{3}}$	**3**	$-\frac{5}{3}$
6	$\overline{\mathbf{3}}$	**15**	$+\frac{1}{3}$
6	**3**	**8**	$-\frac{5}{6}$
6	**3**	**10**	$+\frac{2}{3}$

Table 2.2 Evaluation of the color potential in Eq. (2.31) for all possible interaction channels between fermions in 6-plet and triplet representations. In our convention a negative potential denotes an attractive force.

What can be concluded from Eq. (2.31) is that the force becomes the more attractive the more the color is reduced by the combined state.
We can now ask the question what happens if we add an additional vector-like fermion, such as for example a 6-plet, to the particle content of the Standard Model. This newly introduced particle could then interact by exchange of a gluon with an other 6-plet fermion (anti-fermion) or with an ordinary triplet quark (anti-quark). The according tensor product decomposition then yields the following possible color combinations for the combined state

$$\begin{aligned} \mathbf{6} \otimes \overline{\mathbf{6}} &= \mathbf{1} \oplus \mathbf{8} \oplus \mathbf{27} \ , \\ \mathbf{6} \otimes \mathbf{6} &= \mathbf{6} \oplus \mathbf{15} \oplus \mathbf{15'} \ , \\ \mathbf{6} \otimes \overline{\mathbf{3}} &= \mathbf{3} \oplus \mathbf{15} \ , \\ \mathbf{6} \otimes \mathbf{3} &= \mathbf{8} \oplus \mathbf{10} \ . \end{aligned} \tag{2.32}$$

The evaluation of the color potential for all these possible combinations[5] can be found in Tab. 2.2. It appears that there are multiple attractive channels. Therefore naturally the question arises which channel would form a condensate if the strong interaction becomes non-perturbative.
An answer to this question is suggested by Raby et al. [31]. They proposed that a condensate forms in the most attractive channel (MAC) when the coupling of the theory grows strong. In the given example this means that a 6-plet and anti-6-plet form a condensate which is a color singlet state. Hence, the condensate does not carry color charge and therefore cannot

[5]The tensor product decomposition was performed using the mathematica package LieART.

break the color gauge group. This is a necessary requirement to the proposed model, since a breaking of the gauge group would render massive gluons.
Luckily, the preceding statement is true for all higher dimensional representations that are considered within this thesis. Therefore, we can assume that a condensate of a high color fermion is a singlet. Thus, the gauge group $SU(3)$ is not broken.

2.4 Effective Action for Composite Operators

Properties of a quantum field theory can be described by its correlation functions (Green's functions). Thus, it is important to have a formalism which allow their derivation.
Many methods in field theories are based on perturbative expansions. Nevertheless, there are effects which cannot be described in perturbation theory as for instance dynamical chiral symmetry breaking. Therefore it is necessary to find a method that additionally include the non-linear characteristics of a quantum field theory.
Such a technique is provided by the effective action formalism. Here, one introduces a generating functional $\Gamma(\phi_c)$ for the one-particle irreducible n-point functions, which depend on the expectation value ϕ_c of some quantum field ϕ [11, 32].
However, within the process of dynamical chiral symmetry breaking, it is not a single field that obtains an expectation value, but the composite operator of two fields. This is why it is convenient to introduce an effective action for composite operators $\Gamma(\phi_c, G)$ that also depends on the propagator $G(x, y)$, which is the expectation value of the operator $T\phi(x)\phi(y)$. Originally, this idea was introduced by Cornwall, Jackiw and Tomboulis [33], thereby providing a generalization of the generating functional $\Gamma(\phi_c)$.
We will introduce the basic principles of the effective action formalism for composite operators in the following. For the sake of simplicity, we consider a spinless field ϕ for the following discussion and comment on the generalization to fermion and gauge boson fields later.
We begin with the generating functional $\mathcal{Z}$, which is already familiar from Sec. 2.2.2, but is now extended to include not only local sources $J(x)$ but also bilocal sources $I(x, y)$

$$\begin{aligned}\mathcal{Z}(J, I) &= \exp(i\mathcal{W}(J, I)) \\ &= \int \mathcal{D}[\phi] \exp\left(-S(\phi) + \int d^4x \phi(x) J(x) + \int d^4x d^4y \phi(x)\phi(y) I(x, y)\right) .\end{aligned} \tag{2.33}$$

In this definition $\mathcal{W}(J, I)$ is the generating functional for connected Green's functions and the whole expression is normalized to $\mathcal{Z}[0, 0] = 1$. The action of the theory $S(\phi)$, can be written as

$$S(\phi) = -\int d^4x d^4y \phi(x) G_0^{-1}(x - y)\phi(y) + S_{\text{int}}(\phi) , \tag{2.34}$$

with the free propagator $G_0(x-y)$ and the interacting part $S_{\rm int}$ of the action. Furthermore, defining

$$\begin{aligned}\frac{\delta\mathcal{W}(J,I)}{\delta J(x)} &= \phi_c(x)\,,\\ \frac{\delta\mathcal{W}(J,I)}{\delta I(x,y)} &= \phi_c(x)\phi_c(y) - iG(x,y)\,,\end{aligned} \tag{2.35}$$

the effective action is given by a double Legendre transform of $\mathcal{W}(J,I)$

$$\begin{aligned}\Gamma(\phi_c,G) =& \mathcal{W}(J,I) - \int d^4x\phi_c(x)J(x) - \int d^4xd^4y\phi_c(x)\phi_c(y)I(x,y)\\ &+ i\int d^4xd^4yG(x,y)I(x,y)\,.\end{aligned} \tag{2.36}$$

Eq. (2.35) together with Eq. (2.36) imply that the variation of the effective action with respect to ϕ_c and G is given by

$$\begin{aligned}\frac{\delta\Gamma(\phi_c,G)}{\delta\phi_c(x)} &= -J(x) - 2\int d^4y\phi_c(y)I(x,y)\,,\\ \frac{\delta\Gamma(\phi_c,G)}{\delta G(x,y)} &= iI(x,y)\,.\end{aligned} \tag{2.37}$$

Since the physical state corresponds to vanishing sources, one arrives at the stationary conditions

$$\frac{\delta\Gamma(\phi_c,G)}{\delta\phi_c(x)} = 0\,, \qquad \frac{\delta\Gamma(\phi_c,G)}{\delta G(x,y)} = 0\,. \tag{2.38}$$

Since the effective action $\Gamma(\phi_c,G)$ is the generating functional for two-particle irreducible Green's functions[6], it can be derived by a series expansion. The result of the expansion is given by

$$\Gamma(\phi_c,G) = S(\phi_c) - \frac{i}{2}\mathrm{Tr}\,\ln G_0^{-1}G + \frac{i}{2}\mathrm{Tr}\,\mathcal{G}^{-1}(\phi_c)G - \frac{i}{2}\mathrm{Tr}\,1 + \Gamma_2(\phi_c,G)\,, \tag{2.39}$$

where $\mathcal{G}^{-1}(\phi_c)$ is the functional operator

$$\mathcal{G}^{-1}(\phi_c) = -\frac{\delta^2 S(\phi_c)}{\delta\phi_c(x)\phi_c(y)} = G_0^{-1}(x-y) - \frac{\delta^2 S_{\rm int}(\phi_c)}{\delta\phi_c(x)\phi_c(y)}\,, \tag{2.40}$$

and $\Gamma_2(\phi_c,G)$ is the sum of all two and higher loop two-particle irreducible vacuum diagrams. For a proof of Eq. (2.39), we refer the reader to [32, 33].

[6] A two-particle irreducible Feynman diagram is one which cannot be divided into two separate diagrams by cutting two lines.

Usually, one is only interested in translation invariant solutions where ϕ_c is a constant and $G(x,y)$ is merely a function of $x-y$. Thus, one can define the effective potential

$$\Gamma(\phi_c, G) = -V(\phi_c, G) \int d^4x \,, \tag{2.41}$$

for which the stationary conditions of Eq. (2.38) are valid as well. Finally, carrying out a Fourier transform yields the following expression

$$\begin{aligned} V(\phi_c, G) =& U(\phi_c) + \frac{i}{2} \int \frac{d^4p}{(2\pi)^4} \mathrm{Tr}\, \ln G_0^{-1}(p) G(p) \\ & - \frac{i}{2} \int \frac{d^4p}{(2\pi)^4} \mathrm{Tr}\, \left[\mathcal{G}^{-1}(\phi_c, p) G(p) - 1 \right] + V_2(\phi_c, G) \,, \end{aligned} \tag{2.42}$$

with the classical potential $U(\phi_c)$ and the sum of all two-particle irreducible vacuum graphs $V_2(\phi_c, G)$, containing the full propagator G. This is also known as the CJT effective potential [33].

Coming back to QCD, it has to be considered how this result changes in a theory with fermions and gauge bosons. The contributions from gauge bosons are of the same kind as shown in Eq. (2.42), but additionally include the Lorentz indices μ and ν. In the case of fermions, one has to consider Fermi statistics. Thus, all factors $1/2$ have to be replaced by -1.

In the following, the full fermion and gauge boson propagators are denoted by $S(p)$ and $D_{ij}^{\mu\nu}(p) = \delta_{ij} D^{\mu\nu}(p)$, respectively and the free propagators are labeled by an index 0. In the process of dynamical chiral symmetry breaking, one does not expect any of the single fields to obtain a vacuum expectation value in the absence of sources.

Due to this, the CJT effective potential depends only on the propagators and is given by

$$\begin{aligned} V(S, D) = & -i \int \frac{d^4p}{(2\pi)^4} \mathrm{Tr} \left[\ln \left(S_0^{-1}(p) S(p) \right) - S_0^{-1}(p) S(p) + 1 \right] \\ & - \frac{i}{2} \int \frac{d^4p}{(2\pi)^4} \mathrm{Tr} \left[- \ln \left(D_{0,\mu\sigma}^{-1}(p) D_{\sigma\nu}(p) \right) + D_{0,\mu\sigma}^{-1}(p) D_{\sigma\nu}(p) - g_{\mu\nu} \right] + V_2(S, D) \,. \end{aligned} \tag{2.43}$$

With this result, the basic principle of the formalism is the following. The CJT potential is an effective potential that depends on the propagators of the theory. The variation with respect to a propagator yields the corresponding Dyson-Schwinger equation, which is the quantum equation of motion. Though, the Dyson-Schwinger equation can have multiple solutions. By the insertion of these solutions into the effective potential it is possible to

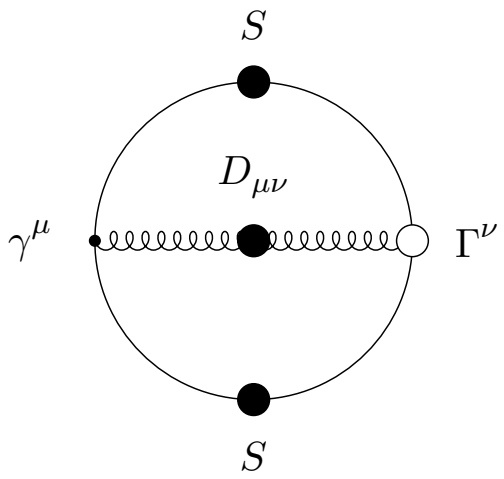

Figure 2.3 The only 2-PI vacuum bubble, contributing to the variation of $V_2(S, D)$ with respect to S. The thick circles represent full propagators and vertices, respectively.

determine the stable minimum, i.e. the true physical solution.
In the considered case, the two stationary conditions are given by

$$\begin{aligned} \frac{\delta V(S,D)}{\delta S} &= 0 \\ \frac{\delta V(S,D)}{\delta D} &= 0\,. \end{aligned} \tag{2.44}$$

For the beginning, we focus on the first stationary condition. To evaluate the functional derivative with respect to S, one first needs to know the 2-PI vacuum graphs which give contributions to $\delta V_2(S, D)/\delta S$. Simply speaking, a derivative with respect to S can be visualized by the process of cutting a fermion line in a Feynman diagram. If there is no such line in the diagram, the derivative vanishes. Therefore, one only needs to regard those graphs including at least one propagator S.
Since it is not possible to include all 2-PI vacuum bubbles in the analysis, one has to stick to some approximation scheme. In this case, the Hartree-Fock approximation is applied which means only retaining those contributions to $V_2(S, D)$ that are lowest order in the coupling constant [33, 34].
Putting all together, there is only one Feynman graph, which contributes within the chosen approximation. Its illustration can be seen in Fig.2.3 . The full propagators S and D are explicitly highlighted by thick black circles, while free propagators will be indicated by bare lines in the succeeding. Furthermore, the diagram has one bare vertex (black dot) and one full vertex Γ_ν(white circle) to prevent double counting of diagrams[34]. The contribution from this diagram is given by

$$V_2(S,D) = i\frac{g^2}{2}\int \frac{d^4p}{(2\pi)^4}\frac{d^4k}{(2\pi)^4}\mathrm{Tr}\left[\gamma_\mu T^i_{\mathbf{R}} S(p)\Gamma^j_\nu(k,p)S(k)D^{\mu\nu}_{ij}(p-k)\right]. \tag{2.45}$$

Following from the Feynman rule in Eq. (2.28), each vertex includes a generator of the representation. Therefore, we introduce the condensed notation $\Gamma^j_\nu = \Gamma_\nu T^j_{\mathbf{R}}$ for the full

vertex. Ultimately, demanding that $V(S, D)$ is stationary against variations of S yields the equation

$$S^{-1}(p) = S_0^{-1}(p) + ig^2 C_2(\mathbf{R}) \int \frac{d^4k}{(2\pi)^4} \gamma_\mu S(k) \Gamma_\nu(k,p) D^{\mu\nu}(p-k)\,. \tag{2.46}$$

The Casimir invariant in above equation arises due to the given color structure of vertices and gluon propagator

$$\delta_{ij} T^i_{\mathbf{R}} T^j_{\mathbf{R}} = \sum_{i=1}^{8} T^i_{\mathbf{R}} T^i_{\mathbf{R}} = C_2(\mathbf{R})\,. \tag{2.47}$$

It should be emphasized that by this, Eq. (2.46) explicitly depends on the representation $\mathbf{R}$ of the participating fermion. The obtained equation is known as the Dyson-Schwinger equation for the fermion propagator. Its pictographic representation can be seen in Fig. 2.4. Besides the fermion DSE, an equation for the gluon propagator can as well be derived using the second stationary condition in Eq.(2.44). In its simplest form, the presented formalism only includes a functional dependence on the gluon and fermion propagator. Though in general, within the generating functional formalism one can derive Dyson-Schwinger equations for every n-point correlation function. Together, they build an infinite tower of coupled differential equations which relate the correlation functions of a theory with each other. This is a remarkably powerful tool, since not only the perturbative effects of QCD are incorporated but also the non-perturbative ones. Nevertheless, in studying the equations one always has to stick to some truncation scheme.

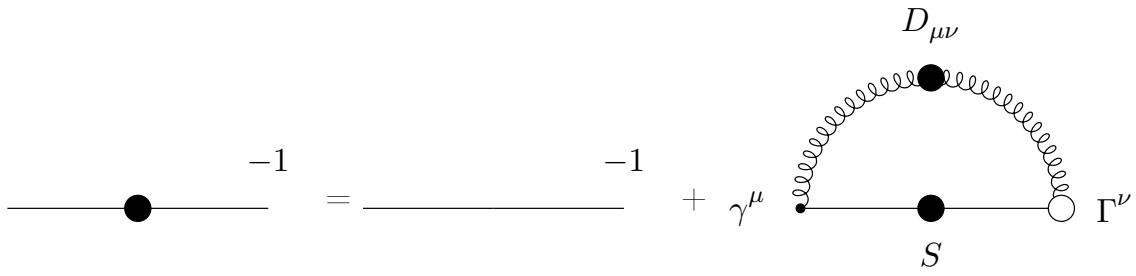

Figure 2.4 Graphical illustration of the Dyson-Schwinger equation for the fermion propagator.

2.5 Renormalization

During the evaluation of specific Feynman diagrams one encounters divergent integrals which need to be regularized. This can be done by introducing a regularization parameter Λ such as for example a momentum cut-off. As a consequence, correlation functions that are calculated from the regularized expressions artificially depend on this parameter Λ. However, physical quantities should not depend on the specific regularization procedure.

In renormalizable theories such as QCD [35], this problem can be cured by introducing a finite number of renormalization constants Z_i which absorb the occurring divergences. By this, dependencies on Λ are removed and physical quantities are instead defined at the renormalization scale μ. Therefore, the Z_i are generally functions of the regularization parameter Λ and the renormalization point μ.
For the renormalization of QCD the bare fields, coupling constant and mass are rescaled according to

$$\begin{aligned} \psi = \sqrt{Z_2}\psi_R\,, \qquad G^\mu = \sqrt{Z_3}G^\mu_R\,, \qquad c = \sqrt{\tilde{Z}_3}\,c_R\,, \\ g_0 = Z_g g_R\,, \qquad m_0 = Z_m m_R\,, \end{aligned} \tag{2.48}$$

where the index R labels renormalized quantities [21]. Additionally, there are the renormalization constants Z_{1F}, Z_1, Z_4 and $\tilde{Z}_1$ for the quark-gluon, three-gluon, four-gluon and ghost-gluon vertices. These quantities are related, by the Slavnov-Taylor identities (STI) [36], which can be derived from BRST invariance [23, 24]:

$$Z_{1F} = Z_g Z_2 Z_3^{1/2}\,, \qquad Z_1 = Z_g Z_3^{3/2}\,, \qquad Z_4 = Z_g^2 Z_3^2\,, \qquad \tilde{Z}_1 = Z_g \tilde{Z}_3\, Z_3^{1/2}\,. \tag{2.49}$$

Since in Landau gauge $\tilde{Z}_1 = 1$, the quark-gluon vertex renormalization factor simplifies to $Z_{1F} = Z_2/\tilde{Z}_3$ [36]. The renormalization constants also transfer to the propagators of the theory. In terms of the bare propagators, they are expressed as

$$\begin{aligned} S_R(p) &= Z_2^{-1} S(p)\,, \\ D^{\mu\nu}_R(p) &= Z_3^{-1} D^{\mu\nu}(p)\,, \\ D^{\text{ghost}}_R(p) &= \tilde{Z}_3^{-1} D^{\text{ghost}}(p)\,, \end{aligned} \tag{2.50}$$

where D^{ghost} denotes the bare ghost propagator. Since from now on all quantities will solely denote the renormlized ones, we suspend with the R from now.
From Eq. (2.46) and the above definitions, we finally arrive at the renormalized DSE for the fermion propagator

$$S^{-1}(p) = Z_2\left(\not{p} - Z_m m\right) - \Sigma'(p)\,, \tag{2.51}$$

with Σ' given by

$$\Sigma'(p) \equiv iC_2(\mathbf{R}) Z_{1F} g^2 \int \frac{d^4k}{(2\pi)^4} \gamma_\mu S(k) \Gamma_\nu(k,p) D^{\mu\nu}(p-k)\,. \tag{2.52}$$

For the following, it is convenient to parameterize the full quark propagator in terms of the Dirac scalar and vector components by

$$\begin{aligned} S^{-1}(p) &= \not{p} - m - \Sigma(p) \\ &\equiv A(p^2)\not{p} - B(p^2) \\ &\equiv Z^{-1}(p^2)\left[\not{p} - M(p^2)\right]\,, \end{aligned} \tag{2.53}$$

where $\Sigma(p)$ is the fermion self-energy, not to be confused with $\Sigma'(p)$.
Besides, it is common to introduce the vector and scalar dressing functions $A(p^2)$ and $B(p^2)$. From these, one can define the quark wave function renormalization $Z(p^2) \equiv 1/A(p^2)$ and the mass function $M(p^2) \equiv B(p^2)/A(p^2)$.
The full gluon propagator in Landau gauge is given by

$$D^{\mu\nu}(p) = \frac{1}{p^2}\left(g^{\mu\nu} - \frac{p^\mu p^\nu}{p^2}\right)\frac{1}{1+\Pi(p^2)}\,, \tag{2.54}$$

where $\Pi(p^2)$ is the gluon self-energy and the factor $1/(1+\Pi(p^2)$ is usually called the gluon dressing function. At the renormalization point μ, the boundary (renormalization) conditions are given by

$$\begin{aligned} S^{-1}(p)\,|_{p=\mu} &\simeq \not{p} - m \\ D^{\mu\nu}(p)\,|_{p=\mu} &\simeq \frac{1}{p^2}\left(g^{\mu\nu} - \frac{p^\mu p^\nu}{p^2}\right). \end{aligned} \tag{2.55}$$

Thus, at the scale $p = \mu$ the fermion and gluon self-energies both vanish, i.e. $\Sigma(p=\mu) = 0$ and $\Pi(p=\mu) = 0$.

2.6 Perturbative Methods in QCD

The DSEs are a suitable tool for investigating both non-perturbative and perturbative effects of QCD. Nonetheless, in the following we will turn to a method that provides a description of the perturbative dynamics of QCD alone. Namely, we will examine the renormalization group equations (RGEs) for the coupling constant and explicit mass. This should provide a better understanding of the large momentum behaviour of these quantities.

2.6.1 Running Coupling Constant

The RGE for the coupling constant originates from the starting assumption that the bare coupling g_0 must be independent of the renormalization point μ and hence

$$0 = \mu\frac{\partial g_0}{\partial\,\mu}\,. \tag{2.56}$$

From this general ansatz one can deduce a differential equation for the renormalized coupling g that is commonly known as the β-function. To one-loop order, the derivation of the β-function includes the evaluation of the vacuum polarization graphs shown in Fig. 2.1. With these, the one-loop running coupling is described by [32, 26]

$$\beta(g) \equiv \mu\frac{\partial g}{\partial\,\mu} = -\frac{b}{2}g^3\,, \tag{2.57}$$

where b is the first coefficient in the expansion in powers of the coupling. Solving this equation yields

$$g^2(p^2) = \frac{2}{b \ln\left(p^2/\Lambda^2_{QCD}\right)}\,, \tag{2.58}$$

with Λ^2_{QCD} the IR scale parameter of QCD that can be calculated from a reference scale M^2, where the coupling is known according to

$$\Lambda^2_{QCD} = M^2 \exp\left(-\frac{2}{b g^2(M^2)}\right). \tag{2.59}$$

In the Standard Model, the coefficient b is given by

$$b = \frac{1}{8\pi^2}\left(\frac{11}{3}C_2(\mathbf{8}) - \frac{2}{3}n_{\mathrm{F}}\right), \tag{2.60}$$

where n_F denotes the number of active quarks[7]. This yields $b = 7/(8\pi^2)$ for $n_F = 6$ active quark flavors. Since $b > 0$, Eq. (2.58) demonstrates that the coupling constant decreases with increasing momentum. Hence, the theory is asymptotic free. Furthermore, we notice that the maximum number of triplet quarks which could be added without destroying the asymptotic freedom is $n_F = 16$.

We want to turn now to the question, how fermions in a high color representation contribute to the running coupling constant. Generally, at one loop the additional contribution of a vector-like fermion in representation $\mathbf{R}$ is described by [37]

$$b^{\mathbf{R}} = -\frac{1}{8\pi^2}\left(\frac{4}{3}T(\mathbf{R})\prod_{i=1,2} d_i(\mathbf{R})\right), \tag{2.61}$$

with the Dynkin index $T(\mathbf{R})$ of the $SU(3)$ representation and the index $i = 1, 2$ symbolizing the $U(1)_Y$ and $SU(2)_L$ gauge group. Thus, $d_i(\mathbf{R})$ labels the dimension of the representation in $U(1)_Y$ and $SU(2)_L$ space, respectively. We note that this expression is generally valid if the factor $\frac{4}{3}$ is substituted by $-\frac{11}{3}$ for gauge bosons, $\frac{2}{3}$ for chiral fermions and $\frac{1}{3}$ for complex scalars. Following from this, the addition of n_V active vector-like fermions that are singlets under the electroweak gauge group leads to the new coefficient

$$b^{\mathrm{new}} = \frac{1}{8\pi^2}\left(\frac{11}{3}C_2(\mathbf{8}) - \frac{2}{3}n_{\mathrm{F}} - \frac{4}{3}T(\mathbf{R})\,n_V\right). \tag{2.62}$$

Using the Dynkin indices from Tab. 2.1, we find the coefficients b^{new} listed in Tab. 2.3 for the lowest dimensional representations. As a result of the rapidly increasing Dynkin indices,

[7] A quark contributes to the running coupling for momenta higher than the threshold of pair production, i.e. $(2m)^2 < p^2$ (see Fig. 2.1a)

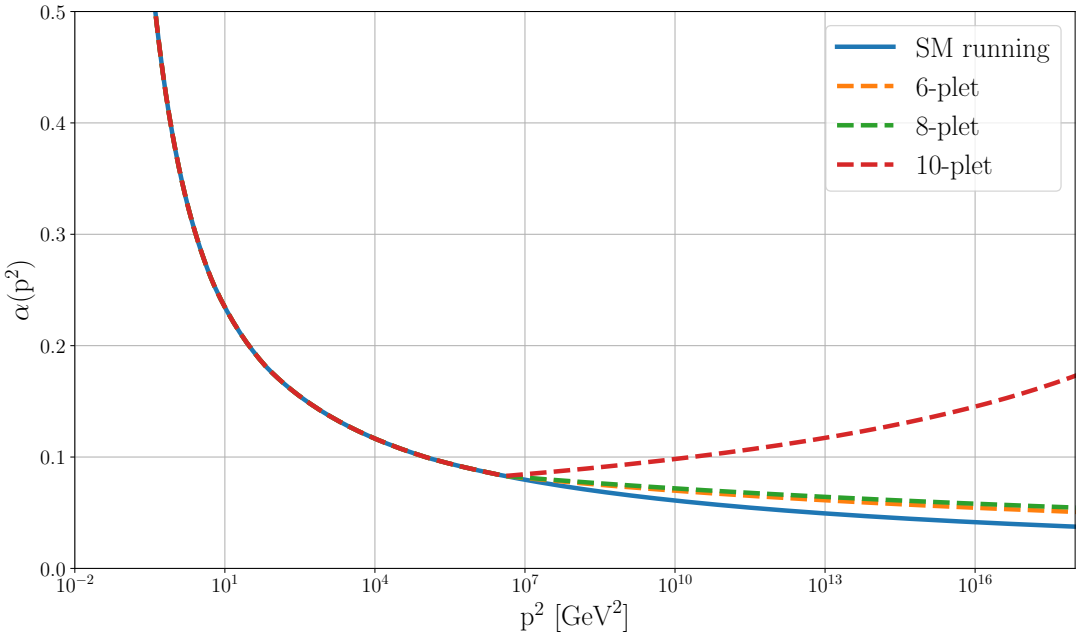

Figure 2.5 The one-loop running coupling $\alpha(p^2)$ for the case of the Standard Model particle content (blue line) and for the case of one additional vector-like fermion with an exemplary mass of 1 TeV in a higher dimesional representation of $SU(3)$.

asymptotic freedom is already lost by adding an additional 10-plet fermion. However, the supplement of one 8-plet or up to two 6-plets would not destroy this characteristic feature of QCD.

For our following analysis, we calculate the perturbative running coupling at one-loop for the Standard Model particle content. For this, we explicitly include the changing value of b at the thresholds of the three heaviest quarks charm, bottom and top[8]. The threshold of the three lightest quarks are of minor significance for our later studies and are therefore not included. As a reference point for our calculation, we use the coupling at the mass of the Z boson $\alpha(M_Z^2) = 0.118$ with $M_Z = 91.2\,\text{GeV}$ [27]. Within this calculation, the IR divergence is located at $\Lambda_{\text{QCD}} = 0.157$ GeV.

An illustration of the behavior of $\alpha(p^2) \equiv 4\pi g^2(p^2)$ within the Standard Model is given by the blue line in Fig. 2.5. Additionally, we show the changed behaviour of the running coupling if we include the additional contribution of one vector-like fermion in a high color representation with an exemplary mass of 1 TeV.

[8] At the particle thresholds, one faces discontinuities in the slope of the running coupling. Therefore, Λ^2_{QCD} is promoted to a variable that depends on the number of active particles, in order to make $g^2(p^2)$ a smooth function of p^2

		$8\pi^2 b^{\text{new}}$	
Rep (R)	$T(R)$	$n_V = 1$	$n_V = 2$
6	5/2	11/3	1/3
8	3	3	−1
10	15/2	−3	−13
15	10	−19/3	−59/3

Table 2.3 First coefficient b^{new} of the beta function for the strong coupling constant, including the effects of n_V additional vector-like fermions in representation $\mathbf{R}$ of $SU(3)$. In our convention, a negative value indicates loss of asymptotic freedom.

2.6.2 Running Mass

Until now, a clear description of the running coupling in the one-loop approximation was developed. We will adopt this knowledge to investigate the pure perturbative running of an explicit chiral symmetry breaking mass. As a reminder from the previous section, the bare mass m_0 is related to the renormalized mass by the renormalization constant

$$m_0 = Z_m(\Lambda^2, \mu^2) m(\mu^2)\,, \tag{2.63}$$

where for clearness all dependencies on the cut-off scale Λ and the renormalization scale μ are indicated explicitly. Proceeding in a similar way as before, we start by introducing the anomalous mass dimension

$$\gamma_m(g^2) \equiv \mu \frac{\partial \ln Z_m(\Lambda^2, \mu^2)}{\partial \mu}\,. \tag{2.64}$$

To one-loop order, the derivation of γ_m includes the evaluation of the fermion self energy, illustrated in Fig. 2.6, which yields $\gamma_m(g^2) = cg^2$ with $c = \frac{3}{8\pi^2} C_2(\mathbf{R})$ [38]. With this knowledge and additionally taking into account the β-function for the running coupling in Eq. (2.57), we can solve Eq. (2.64) to obtain an expression for the renormalization constant

$$Z_m(\Lambda^2, \mu^2) = \left[\frac{\ln\left(\mu^2/\Lambda^2_{QCD}\right)}{\ln\left(\Lambda^2/\Lambda^2_{QCD}\right)} \right]^{d_m}\,, \tag{2.65}$$

where we defined the quantity

$$d_m \equiv \frac{c}{b} = \frac{3C_2(\mathbf{R})}{\frac{11}{3}C_2(\mathbf{8}) - \frac{2}{3}n_{\mathrm{F}} - \frac{4}{3}T(\mathbf{R})\, n_V}\,. \tag{2.66}$$

As outlined in the previous section, this includes only the contributions of active particles within the considered momentum range.

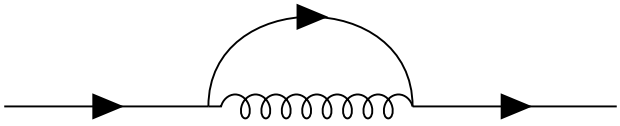

Figure 2.6 Graphical illustration of the one-loop self-energy of the fermion propagator in QCD.

Since the left side of Eq. (2.63) is independent of μ, we can relate the masses at two scales by the ratio of the renormalization constants which finally yields

$$m(p^2) = m(\mu^2) \left[\frac{\ln\left(\mu^2/\Lambda_{QCD}^2\right)}{\ln\left(p^2/\Lambda_{QCD}^2\right)} \right]^{d_m} . \tag{2.67}$$

This analysis demonstrates that the explicit chiral symmetry breaking mass is subject to a logarithmic running in the UV that is determined by the behavior of the perturbative running coupling. Since this equation applies to all scales the expression

$$\hat{m} \equiv m(\mu^2) \left[\ln\left(\mu^2/\Lambda_{QCD}^2\right) \right]^{d_m} , \tag{2.68}$$

denotes a renormalization group invariant quantity which can be understood as the mass analogue to Λ_{QCD}.

2.7 Operator Product Expansion

In the previous section, we considered perturbative methods which provide a description for the large momentum behaviour of the explicit chiral symmetry breaking mass m. We will now investigate what can be said about the UV asymptotics of the complete dynamical mass function $M(p^2)$. In order to do so, we start by introducing the formal definition of the fermion condensate.

Rigorously, the bare fermion condensate is defined as the expectation value of the normal-ordered local operator product with respect to the full non-perturbative vacuum $|\text{vac}\rangle$ [29]

$$\langle\overline{\psi}\psi\rangle_0 \equiv -\lim_{x\to 0} \text{Tr}\langle\text{vac}| : \overline{\psi}(0)\psi(x) : |\text{vac}\rangle , \tag{2.69}$$

where exceptionally the fermion fields in above equation should denote the bare ones and the trace is over both color and Dirac space[9]. We note that the normal-ordering in above equation should be understood with respect to the perturbative vacuum $|0\rangle$. Then by definition the fermion condensate vanishes to all orders in perturbation theory, i.e. $\langle 0| : \overline{\psi}(0)\psi(x) : |0\rangle = 0$. Thus, it is purely the result of the non-perturbative dynamics of

[9] Note, that we chose a different sign convention than the one used in [29] so that the value of the chiral condensate is positive.

QCD.
Since the renormalization constant for the composite operator is given by [39]

$$(\overline{\psi}\psi)_0 = Z_m^{-1}(\Lambda^2, \mu^2)\,(\overline{\psi}\psi)_\mu\,, \tag{2.70}$$

Eq. (2.69) can be rewritten in terms of renormalized operators and fields, which leads to an expressions for the renormalized condensate, given by

$$\langle\overline{\psi}\psi\rangle_\mu = -Z_2(\Lambda^2, \mu^2)Z_m(\Lambda^2, \mu^2)\lim_{x\to 0}\mathrm{Tr}\langle\mathrm{vac}|:\overline{\psi}(0)\psi(x):|\mathrm{vac}\rangle\,. \tag{2.71}$$

Though we note, the factor Z_2 can be neglected when considering the large momentum behavior, since the perturbative one-loop calculation in Landau gauge yields $Z_2(\Lambda^2, \mu^2) = 1$.

A suitable tool to describe the short distance behavior of composite operators is the operator product expansion which was originally introduced by Wilson [40].
The general concept starts from the fact that the time-ordered product of two local operators A and B can be expanded by a sum

$$TA(x)B(y) = \sum_i C_i\left((x-y)^2\right)N_i(x,y)\,, \tag{2.72}$$

where $C_i\left((x-y)^2\right)$ are the Wilson coefficients that are singular in $x \to y$ and $N_i(x,y)$ are bilocal normal-ordered operators which are regular in the limit $x \to y$ [29]. To explore the above expression in the limit $x \to y$ it is sufficient to consider a basis for the N_i which is given by all operators that have the same transformation properties and quantum numbers as the product $A(x)B(y)$. Hence, with respect to the composite operator of two fermion fields, a basis is given by gauge invariant and scalar operators such as for example

$$\mathbf{1}\,,\ :\overline{\psi}(0)\psi(x):,\ :\overline{\psi}(0)\not{D}\psi(x):,\ \ldots\,. \tag{2.73}$$

We will apply this to investigate the large momentum behavior of the fermion propagator that is defined by $S(x) \equiv -i\langle\mathrm{vac}|T\psi(x)\overline{\psi}(0)|\mathrm{vac}\rangle$.
Following the considerations of Lane and Politzer [38, 41], the expansion in the two lowest dimensional operators $\mathbf{1}$ and $:\overline{\psi}(0)\psi(x):$ is given by

$$\langle\mathrm{vac}|T\psi(x)\overline{\psi}(0)|\mathrm{vac}\rangle \overset{x\to 0}{\simeq} \left[i\gamma_\mu\partial_\mu C_0(x^2) + m(\mu^2)C_1(x^2)\right]\langle\mathbf{1}\rangle + C_2(x^2)\langle\overline{\psi}\psi\rangle_\mu + \ldots\,, \tag{2.74}$$

where we applied the definition of the condensate. The Fourier transform of above equation can now be compared to the expansion of the fermion propagator in Eq. (2.53) for large momenta

$$S(p) \overset{p\to\infty}{\simeq} \frac{1}{A(p^2)}\left[\frac{\not{p}}{p^2} + \frac{1}{p^2}M(p^2) + \ldots\right]\,. \tag{2.75}$$

This leads to the following identifications

$$\frac{-i}{p^2 A(p^2)} = C_0(p^2)\,, \tag{2.76}$$

$$\frac{i}{p^2 A(p^2)} M(p^2) = m(\mu^2) C_1(p^2) + \langle\overline{\psi}\psi\rangle_\mu C_2(p^2)\,, \tag{2.77}$$

with the Fourier transformed Wilson coefficients $C_i(p^2) = \int d^4x e^{ipx} C_i(x^2)$. At present, from purely dimensional analysis we already expect the momentum dependencies $C_1(p^2) \sim 1/p^2$ and $C_2(p^2) \sim 1/(p^2)^2$. The exact behavior of the Wilson coefficients can be obtained by the analysis of the corresponding renormalization group equations with boundary conditions that originate from the evaluation of the short distance limit $x \to 0$ in the Green's function $\langle \text{vac}|T\psi(x)\overline{\psi}(0)\psi(y)\overline{\psi}(z)|\text{vac}\rangle$. For details on the derivation, we refer to [32, 41] and quote here the resulting large momentum behaviour of the dynamical mass function in the lowest order approximation

$$M(p^2) \overset{p\to\infty}{\simeq} \underbrace{m(\mu^2)\left[\frac{\ln\left(\mu^2/\Lambda^2_{QCD}\right)}{\ln\left(p^2/\Lambda^2_{QCD}\right)}\right]^{d_m}}_{\text{perturbative}} + \underbrace{\frac{4\pi^2 d_m}{d(\mathbf{R})}\langle\overline{\psi}\psi\rangle_{\text{inv}}\frac{1}{p^2}\left[\ln\left(p^2/\Lambda^2_{QCD}\right)\right]^{d_m-1}}_{\text{non-perturbative}}\,, \tag{2.78}$$

with the renormalization group invariant condensate defined in analogy to the renormalization group invariant mass by

$$\langle\overline{\psi}\psi\rangle_{\text{inv}} \equiv \frac{\langle\overline{\psi}\psi\rangle_\mu}{\left[\ln\left(\mu^2/\Lambda^2_{QCD}\right)\right]^{d_m}}\,, \tag{2.79}$$

and $A(p^2) \to 1$ for large momenta. Since in the upcoming section, we will always denote the explicit mass at the renormalization point μ, we suspend with the explicit notation and simply write $m \equiv m(\mu^2)$.

To close this section, the following concluding remarks are in order. First of all, it is important to stress that the derivation of the OPE does not proof that spontaneous chiral symmetry breaking takes places. It merely provides an expression for the behavior of the dynamical mass function at large momenta if $\langle\overline{\psi}\psi\rangle_{\text{inv}} \neq 0$.

Secondly, we recognize an essential difference between the two terms contributing to Eq. (2.78). While at large momenta, the perturbative running mass is logarithmically decreasing, the non-perturbative condensate decays much more rapidly by $1/p^2$. We will use this key observation in Chapter 4, in order to extract the condensate from the dynamical mass function $M(p^2)$ systematically.

Chapter 3

Truncation of the Fermion Dyson-Schwinger Equation

In the last chapter, the renormalized form of the fermion DSE was derived. Our aim is now to solve this equation and find a solution for the full fermion propagator. Especially, we are interested in the dynamical mass function $M(p^2)$, in order to ascertain the value of the fermion condensate.
As a reminder, we quote here the full form of the fermion DSE as derived in the previous chapter

$$S^{-1}(p) = Z_2\left(\not{p} - Z_m m\right) - iC_2(\mathbf{R})Z_{1F}g^2\int\frac{d^4k}{(2\pi)^4}\gamma_\mu S(k)\Gamma_\nu(k,p)D^{\mu\nu}(p-k)\,. \tag{3.1}$$

From this expression it is evident that the fermion propagator $S(p)$ is part of both sides of the equation. Thus, one needs to solve the equation self-consistently.
The problem in doing so resides in the fact that there are further unknown quantities.
This is on the one hand the full gluon propagator $D^{\mu\nu}(p-k)$ and on the other hand the dressed quark-gluon vertex $\Gamma_\nu(k,p)$.
As a matter of fact, it is the inherent structure of a DSE for a n-point correlation function, that it depends on a (n+1)-point correlation function, which itself is subject to its own DSE. This infinite tower of coupled equations cannot be solved analytically. Thus, it needs to be truncated in some suitable way, which we will elaborate in this chapter.

3.1 Truncation Scheme

First of all we notice that apart from the renormalization constants, Eq. (3.1) has no explicit dependence on ghosts. There is rather an indirect contribution through the dressing function of the gluon propagator and the quark-gluon vertex. The latter is in general constrained by a STI which includes the ghost dressing function and the ghost-quark scattering kernel [11].
In a first attempt to simplify the DSE, we will neglect the contributions of ghosts. This

is a common starting point for the truncation as presumably the effects of ghost can be included by adjusting the phenomenology in the gluon sector [42, 11].
Ignoring the ghost contributions, the STI for the full quark-gluon vertex becomes equal to the Ward-Takahashi identity (WTI) of quantum electrodynamics that is given by [42]

$$q_\mu \Gamma_\mu(k,p) = S^{-1}(k) - S^{-1}(p)\,, \qquad q_\mu = p_\mu - k_\mu\,. \tag{3.2}$$

From studies of the DSE in abelian theories there are ansätze for the dressed quark-gluon vertex which satisfy above WTI. These are for example the Ball-Chiu vertex [43] or the Curtis-Pennington vertex [44].
However, we will stick to an even more simplified ansatz and take the bare vertex approximation

$$\Gamma_\mu(k,p) = \gamma_\mu\,, \tag{3.3}$$

commonly also referred to as the "rainbow approximation" (see e.g. [45]). One should keep in mind that this ansatz does not respect the WTI. Though, investigating the impact of more advanced vertex structure is beyond the scope of this thesis and will be left for future work.
In going on with the truncation, we apply a further approximation which is often named the "abelian approximation" [42, 45]. Here, one replaces the factor

$$Z_{1F} g^2 D^{\mu\nu}(p-k) \longrightarrow 4\pi\alpha_{\text{eff}}\left((p-k)^2\right) D_0^{\mu\nu}(p-k)\,, \tag{3.4}$$

where $D_0^{\mu\nu}$ is the free gluon propagator that is given by

$$D_0^{\mu\nu}(p) = \frac{1}{p^2}\left(g^{\mu\nu} - \frac{p^\mu p^\nu}{p^2}\right)\,. \tag{3.5}$$

In doing so, it is assumed that the non-perturbative effects of the dressed gluon propagator are completely incorporated by an effective running coupling constant, which is phenomenologically motivated[1] . We will give more details on this at a later point.
For now, the fermion DSE can be decoupled from the gluon DSE and solved in its final closed form:

$$\begin{aligned} S^{-1}(p) &= Z_2\left(\not{p} - Z_m m\right) - \Sigma'(p)\,, \\ \Sigma'(p) &= iC_2(\mathbf{R})4\pi \int \frac{d^4k}{(2\pi)^4}\alpha_{\text{eff}}((p-k)^2)\gamma_\mu S(k)\gamma_\nu D_0^{\mu\nu}(p-k)\,. \end{aligned} \tag{3.6}$$

Recalling from the last chapter, we assume that the fermion propagator can be described by its Dirac vector and scalar dressing functions $S^{-1}(p) = A(p^2)\not{p} - B(p^2)$. Thus, in order to gain knowledge about the full fermion propagator we have to solve Eq. (3.6) for the two dressing functions $A(p^2)$ and $B(p^2)$. To do so it is necessary to evaluate the Dirac structure

[1] Note that in our notation g indicated the coupling at the renormalization scale μ, i.e. $g \equiv g(p^2)\,|_{p^2=\mu^2} = 4\pi\alpha(p^2)\,|_{p^2=\mu^2}$.

of the right hand side of the equation.
Suppose, there is a similar decomposition of $\Sigma'(p)$ into a vector and a scalar component

$$\Sigma'(p) \equiv \Sigma'_{\mathrm{v}}(p^2)\not{p} + \Sigma'_s(p^2)\,. \tag{3.7}$$

Then, putting this decomposition into Eq. (3.6) yields

$$A(p^2)\not{p} - B(p^2) = \left[Z_2 - \Sigma'_{\mathrm{v}}(p^2)\right]\not{p} - \left[Z_2 Z_m m + \Sigma'_s(p^2)\right]\,. \tag{3.8}$$

As a result, we are able to identify the vector and scalar parts of each side of the equation from which the following system of coupled equations can be obtained

$$\begin{aligned} A(p^2) &= Z_2 - \Sigma'_{\mathrm{v}}(p^2)\,, \\ B(p^2) &= Z_2 Z_m m + \Sigma'_s(p^2)\,. \end{aligned} \tag{3.9}$$

The functions $\Sigma'_{\mathrm{v}}(p^2)$ and $\Sigma'_s(p^2)$ can be extracted from the whole expression Σ' by projecting out the two different components under usage of a Dirac trace

$$\begin{aligned} \Sigma'_{\mathrm{v}}(p^2) &= \frac{1}{4p^2}\mathrm{Tr}_D\left[\not{p}\Sigma'(p)\right]\,, \\ \Sigma'_{\mathrm{s}}(p^2) &= \frac{1}{4}\mathrm{Tr}_D\left[\Sigma'(p)\right]\,, \end{aligned} \tag{3.10}$$

where the factor $1/4$ is a normalization factor.
Then, using the standard identities for Dirac matrices that are summarized in Appendix A.2, the two relevant traces are given by

$$\begin{aligned} \mathrm{Tr}_D\left[\not{p}\gamma_\mu S(k)\gamma_\nu D_0^{\mu\nu}(p-k)\right] = &-\frac{4}{(p-k)^2}\frac{A(k^2)}{A^2(k^2)k^2 - B^2(k^2)} \\ &\times\left[3(p\cdot k) - \frac{2}{(p-k)^2}\left(p^2k^2 - (p\cdot k)^2\right)\right]\,, \end{aligned} \tag{3.11}$$

$$\mathrm{Tr}_D\left[\gamma_\mu S(k)\gamma_\nu D_0^{\mu\nu}(p-k)\right] = \frac{4}{(p-k)^2}\frac{3B(k^2)}{A^2(k^2)k^2 - B^2(k^2)}\,,$$

exploiting frequently the relation

$$p\cdot k = \frac{k^2 + p^2 - (p-k)^2}{2}\,. \tag{3.12}$$

Next, we have to evaluate the integral over momentum k in Eq. (3.6).
As a start, we perform a Wick rotation to go from Minkowski metric to Euclidean space (see Appendix A.4). Furthermore, reminding that the dressing functions depend solely on p^2 it is convenient to introduce spherical coordinates.
Generally, the integration in d-dimensional space can be rewritten by introducing spherical

angles ϕ and β_j, $j = 1, .., d-2$. Using these new coordinates, the integral can be substituted according to

$$\begin{aligned}\int d^d k &= \int \frac{k^{d-2}}{2} dk^2 d\phi \prod_{j=1}^{d-2} \sin^k(\beta_j) d\beta_j \\ &= \Omega_d \int \frac{k^{d-2}}{2} dk^2 \sin^{d-2}(\beta_{d-2}) d\beta_{d-2}\,,\end{aligned} \tag{3.13}$$

where in the second line the trivial angular dependencies are integrated out and merged together to the quantity Ω_d.
For $d = 4$ one has $\Omega_{d=4} = 4\pi$ so that the overall integration measure becomes $\int d^d k = 2\pi \int k^2 dk^2 \sin^2(\beta) d\beta$, where β is defined as the angle between the four vectors k and p

$$\cos(\beta) = \frac{p \cdot k}{\sqrt{p^2 k^2}}\,. \tag{3.14}$$

We note that $p \cdot k$ denotes now the Euclidean inner product. Finally, putting all together we arrive at the two coupled equations

$$\begin{aligned}A(p^2) = Z_2 + \frac{C_2(\mathbf{R})}{2\pi^2 p^2} \int dk^2 \frac{k^2 A(k^2)}{A^2(k^2)k^2 + B^2(k^2)} \int_0^\pi d\beta \sin^2(\beta) \\ \times \frac{\alpha_{\text{eff}}\left((p-k)^2\right)}{(p-k)^2} \left[3(p\cdot k) - \frac{2}{(p-k)^2}\left(p^2 k^2 - (p\cdot k)^2\right)\right]\,,\end{aligned} \tag{3.15}$$

$$B(p^2) = Z_2 Z_m m + \frac{C_2(\mathbf{R})}{2\pi^2} \int dk^2 k^2 \frac{3B(k^2)}{A^2(k^2)k^2 + B^2(k^2)} \int_0^\pi d\beta \sin^2(\beta) \frac{\alpha_{\text{eff}}\left((p-k)^2\right)}{(p-k)^2}\,, \tag{3.16}$$

which can be solved numerically to find the dressing functions $A(p^2)$ and $B(p^2)$.

3.2 Numerical Treatment

Before starting the evaluation of Eqs. (3.15) and (3.16), we have to introduce an infrared (IR) cut-off η and an ultraviolet (UV) cut-off Λ for the integration in radial direction

$$\int_{\eta^2}^{\Lambda^2} dk^2\,. \tag{3.17}$$

The IR cut-off is chosen sufficiently small so that we assume its effect will be of no significance compared to the whole integral. The UV cut-off Λ is the regularizing parameter of the divergent integral. Its dependence should however drop out later when we apply the

renormalization conditions. Within our analysis we use $[\eta^2, \Lambda^2] = [10^{-4}\,\mathrm{GeV}^2, 10^{24}\,\mathrm{GeV}^2]$.

For the numerical implementation we rewrite the angular part of the integral by a coordinate transformation

$$\int_0^\pi d\beta \sin^2(\beta) = \int_{-1}^1 dz \sqrt{1-z^2}\,, \qquad z \equiv \cos(\beta)\,. \tag{3.18}$$

With Eqs. (3.12) and (3.14) it is now possible to express the integrals by the variables z, p^2 and k^2 only:

$$\begin{aligned} A(p^2) =& Z_2 + \frac{C_2(\mathbf{R})}{2\pi^2 p^2} \int_0^{\Lambda^2} dk^2 \frac{k^2 A(k^2)}{A^2(k^2)k^2 + B^2(k^2)} \int_{-1}^1 dz \sqrt{1-z^2} \\ &\times \frac{\alpha_{\text{eff}}\left(p^2 + k^2 - 2z\sqrt{p^2\,k^2}\right)}{p^2 + k^2 - 2z\sqrt{p^2\,k^2}} \sqrt{p^2\,k^2} \left[z + \frac{2(z\sqrt{p^2} - \sqrt{k^2})(\sqrt{p^2} - z\sqrt{k^2})}{p^2 + k^2 - 2z\sqrt{p^2\,k^2}} \right], \end{aligned} \tag{3.19}$$

$$B(p^2) = Z_2 Z_m m + \frac{C_2(\mathbf{R})}{2\pi^2} \int_0^{\Lambda^2} dk^2 \frac{3\,k^2 B(k^2)}{A^2(k^2)k^2 + B^2(k^2)} \int_{-1}^1 dz \sqrt{1-z^2}\, \frac{\alpha_{\text{eff}}\left(p^2 + k^2 - 2z\sqrt{p^2\,k^2}\right)}{p^2 + k^2 - 2z\sqrt{p^2\,k^2}}\,. \tag{3.20}$$

Furthermore, we use Gaussian quadrature rules to carry out the numerical integration. They are based on the idea of representing an integral on the interval $[-1, 1]$ by a weighted sum of function values at N specific points

$$\int_{-1}^1 W(x) g(x) dx \simeq \sum_{i=1}^N w_i g(x_i)\,. \tag{3.21}$$

Depending on the occurring weighting function, we use different quadrature rules which determine the weigts w_i and evaluation points x_i for some chosen N. The accuracy of this numerical method is increased, the higher the number of evaluation points N. For the study within this thesis, we evaluated the angular integral with $N_z = 100$, whereas for the radial integral we take $N_R = 500$ evaluation points.
Precisely, in case of the radial part of the integral the Gauss-Legendre quadrature is applied, whereas for the angular integral we use the Chebyshev-Gauss quadrature. More details on this including the shift of the integration interval for the radial part can be found in Appendix B.
Conclusively, we discretize the functions A and B on a momentum grid. Since we are

interested in a wide range of momenta, it is convenient to chose a logarithmic spacing for the analysis. To this end, all technical procedures are prepared to find a solution for the fermion DSE by an iteration process adopted from [46]:

1. Start by an initial guess for the discretized dressing functions $A(p^2)$ and $B(p^2)$.

2. Put these into the right hand side of Eqs. (3.19) and (3.20) in order to calculate the left hand side .

3. Calculate the discrepancy between the new values obtained for $A(p^2)$ and $B(p^2)$ and the old values.

4. If the discrepancy is below some requested accuracy, stop iterating. If it is not, go back to the second step and continue with the new obtained values for $A(p^2)$ and $B(p^2)$, till the desired accuracy is achieved.

In order not to bias the results by distinct initial guesses, the starting point of the iteration is always chosen the same, i.e. $A(p^2) = 1$ and $B(p^2) = 0.1$ GeV and the iteration is stopped at an accuracy of one part in 10^{24}.
It is worth to mention that in the chiral limit $m = 0$, Eq. (3.20) always has the trivial solution $B(p^2) = 0$ GeV. If the integrated strength of the effective strong coupling is high enough, there is a second solution with $B(p^2) \neq 0$ GeV. However, using above iteration procedure one only finds the zero solution if the initial guess of $B(p^2)$ is exactly zero. Starting from a non-zero initial guess, the iteration will always find the chiral symmetry breaking solution.

3.3 Boundary Conditions

At this point, we want to explain how the renormalization constants Z_2 and Z_m can be determined in order to realize the boundary conditions of Eq. (2.55).
Again, setting equal the fermion DSE in Eq. (2.51) with the definition of the full fermion propagator of Eq. (2.53) yields

$$Z_2 \left(\not{p} - Z_m m\right) - \Sigma'(p) = \not{p} - m - \Sigma(p)\,. \tag{3.22}$$

To evaluate this equation further, the Dirac structure of $\Sigma(p)$ is decomposed by the same ansatz as done for $\Sigma'(p)$ in Eq. (3.7) .
Plugging this decomposition back in above equation leads to

$$\left[Z_2 - \Sigma'_{\mathrm{v}}(p^2)\right] \not{p} - \left[Z_2 Z_m m + \Sigma'_s(p^2)\right] = \left[1 - \Sigma_{\mathrm{v}}(p^2)\right] \not{p} - \left[m + \Sigma_s(p^2)\right]\,, \tag{3.23}$$

where we can identify the scalar and vector parts of each side of the equation

$$\begin{aligned}\Sigma_{\mathrm{v}}(p^2) &= 1 - Z_2 + \Sigma'_{\mathrm{v}}(p^2)\,,\\ \Sigma_s(p^2) &= Z_2 Z_m m - m + \Sigma'_s(p^2)\\ &= m\left[Z_2 Z_m - 1\right] + \Sigma'_s(p^2)\,.\end{aligned} \tag{3.24}$$

Now employing the boundary conditions from Eq. (2.55) at $p^2 = \mu^2$, we obtain two expressions for the renormalization constants

$$Z_2 = 1 + \Sigma'_{\mathrm{v}}(\mu^2)\,, \qquad Z_m = \frac{1}{Z_2} - \frac{\Sigma'_s(\mu^2)}{Z_2 m}\,. \tag{3.25}$$

Throughout our analysis, we use the renormalization point $\mu^2 = 10^{24}\,\mathrm{GeV}^2$. Physical quantities are fixed at this energy scale and thereby dependencies on the cut-off Λ drop out completely.

3.4 Effective Strong Coupling

Finally, we are left with the question which α_{eff} should be used for the solution of the fermion Dyson-Schwinger equation.
What is known so far is the behavior of the perturbative running coupling of QCD as discussed in Sec. 2.6.1. For sure, the effective coupling α_{eff} should behave like the perturbative running coupling at large momenta. However, we cannot say much about the low momentum regime, where QCD confines and passes over to an effective theory of bound states of fermions. Thus, we are left with the purely phenomenological motivation of providing sufficient strength in the IR for dynamical chiral symmetry breaking to happen. This will be done by simply setting the perturbative running coupling to a constant if some value α_{max} is reached in the IR. Exemplary, the low momentum behavior is illustrated in Fig. 3.1 for the one-loop Standard Model running. Note however, that we employ the same IR truncation if we include the contribution of the new high color fermion to the perturbative running.
For a massless triplet fermion, it is possible to find a chiral symmetry breaking solution if $\alpha_{\mathrm{max}} \gtrsim 1$. Furthermore, we observe that the dynamically generated mass grows with an increasing α_{max}. Thus, we adjust this value so that the generated dynamical mass of a triplet fermion in the chiral limit is roughly at the order of $\sim 100 - 200\,\mathrm{MeV}$. This is achieved for $\alpha_{\mathrm{max}} = 12$.
Other proposals for the effective running coupling are suggested in e.g. [47, 48]. These are explicitly fine tuned to reproduce the pion decay constant and mass. However, since we are interested in the investigation of basic properties of a new mechanism, we stick to the simplest approximation for the beginning.

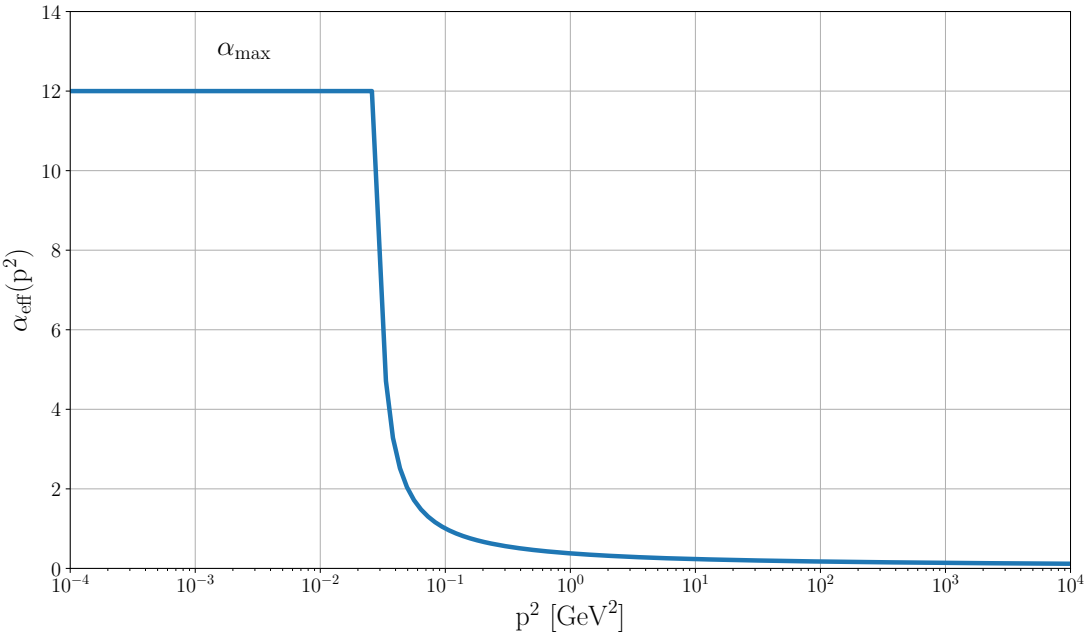

Figure 3.1 Effective running coupling $\alpha_{\text{eff}}(p^2)$ that is cut at a maximum value $\alpha_{\max} = 12$ in the IR.

Chapter 4

Solution of the Fermion Dyson-Schwinger Equation

In the following chapter, we present the solutions of the DSE that we obtained within the truncation scheme described in the previous chapter.
We start by considering the chiral limit with fermions in different representations and show two methods to calculate the expectation value of the condensate. Afterwards, we investigate the characteristics of solutions for massive fermions and propose a method, in order to extract a lower bound for the condensate from the dynamical mass function $M(p^2)$. This is illustrated by the example of a triplet representation. Finally, we generalize the acquired knowledge to massive fermions in higher representations of the color gauge group.

4.1 Solution in the Chiral Limit

To get an impression of the impact of the chosen representation, we start by considering the chiral limit $m = 0$ for a fermion in representation $\mathbf{R} \in \{\mathbf{3}, \mathbf{6}, \mathbf{8}, \mathbf{10}, \mathbf{15}\}$ of the color gauge group, which experiences the effective running coupling, shown in Fig. 3.1.
Remembering from Eq. (3.16), there exist two solutions, one with $M(p^2) = 0$ and one with $M(p^2) \neq 0$. Nevertheless, investigations of the CJT effective potential in [42] (and references therein) have shown, that the ground state with $M(p^2) \neq 0$ is dynamically favored. Thus, what is shown in the following is always the non-zero solution of the Dyson-Schwinger equation.
The wave function renormalization $Z(p^2) = 1/A(p^2)$ and the mass function $M(p^2) = B(p^2)/A(p^2)$ acquired from Eqs. (3.19) and (3.20) can be seen in Fig. 4.1 for the considered representations.
The solution shows a dynamically generated mass with a non-trivial momentum dependence. It has its maximum in the IR and rapidly decreases to zero for higher momenta. Again, we emphasize the fact that although starting from a massless theory, the fermion acquires a mass. Evidently this shows, that dynamical chiral symmetry breaking is present within the

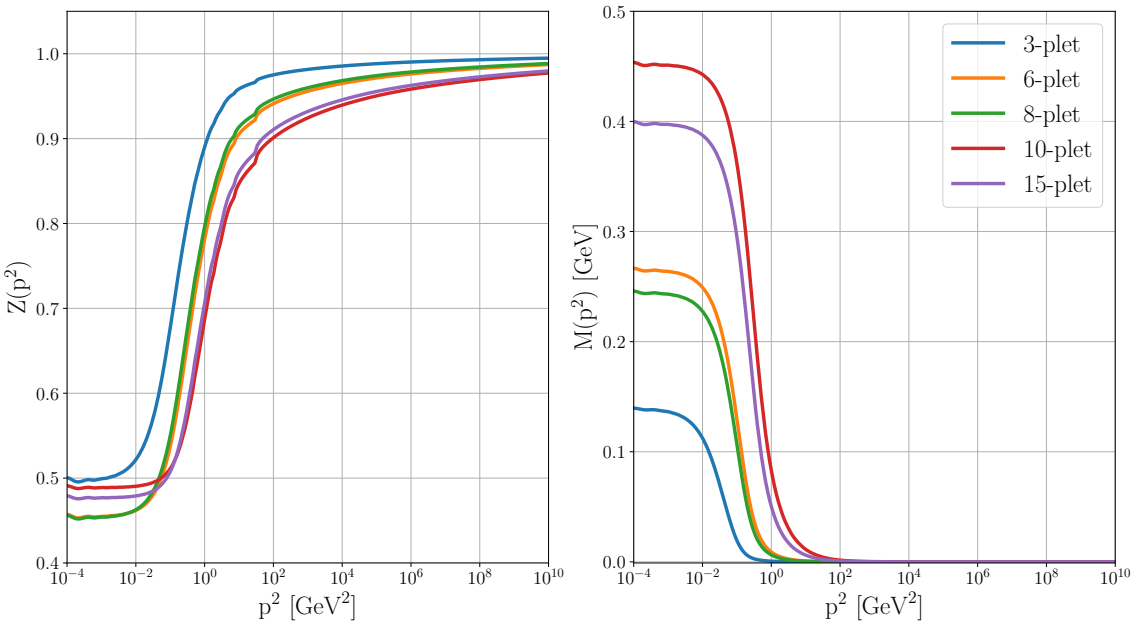

Figure 4.1 Fermion wave function renormalization $Z(p^2)$ (left) and mass function $M(p^2)$ (right) for the chiral limit $m = 0$ with fermions in different representations.

employed truncation. Furthermore, one realizes, that the wave function renormalization $Z(p^2) \to 1$ for large momenta. This is what is expected, since QCD is asymptotic free in the UV and perturbation theory predicts $Z(p^2) = 1$.
Regarding the differences between the representations, the wave function renormalization for higher dimensional representations converges much slower towards the UV limit.
Furthermore the results show, that the dynamically generated mass in the IR increases with increasing Casimir constant. One should remember however, that the Casimir constant is not linearly growing with the dimension of the representation. In particular, the mass function of the 10-plet exceeds that of the 15-plet, due to its higher Casimir constant and the same is true for the 6-plet and 8-plet representation (see Table 2.1).
Additionally we recognize that the mass function for a triplet starts to drop off for momenta $p^2 \gtrsim 10^{-2}\,\mathrm{GeV}^2$, while for the 10-plet, the decrease starts at slightly higher scales of roughly $p^2 \gtrsim 10^{-1}\,\mathrm{GeV}^2$. Conclusively, chiral symmetry is already broken at higher scales for exotic representations.

4.1.1 Chiral Condensate

With these solutions at hand, the next step is to determine the expectation value of the condensate.
In Sec. 2.7, we gave a formal definition for the renormalization point dependent condensate which we repeat here as a reminder

$$\langle\overline{\psi}\psi\rangle_\mu = -Z_2 Z_m \lim_{x\to 0} \mathrm{Tr}\langle \mathrm{vac}| : \overline{\psi}(0)\psi(x) : |\mathrm{vac}\rangle\,. \tag{4.1}$$

In the chiral limit, where the explicit mass is zero, the above expression can be evaluated further using Wicks theorem

$$: \overline{\psi}(0)\psi(x) := T\overline{\psi}(0)\psi(x) - \langle 0|T\overline{\psi}(0)\psi(x)|0\rangle \,, \tag{4.2}$$

and applying the definition of the full, non-perturbative fermion propagator $S(x) \equiv -i\langle \mathrm{vac}|T\psi(x)\overline{\psi}(0)|\mathrm{vac}\rangle$ [49]. The quantity $S_{\mathrm{pert}}(x) \equiv -i\langle 0|T\psi(x)\overline{\psi}(0)|0\rangle$ should be understood, as the perturbative propagator, i.e. a propagator with a mass function $M(p^2)$ equal to zero. Hence, its Dirac trace vanishes and one is left with [11, 50]

$$\langle \overline{\psi}\psi \rangle_\mu = iZ_2 Z_m \lim_{x\to 0} \mathrm{Tr} S(x) \,. \tag{4.3}$$

It is important to keep in mind, that this is only true in the chiral limit. The perturbative propagator of a massive fermion generally has a non-vanishing mass function.
After performing a Fourier transform, Eq. (4.3) turns into

$$\langle \overline{\psi}\psi \rangle_\mu = iZ_2 Z_m \int \frac{d^4k}{(2\pi)^4} \mathrm{Tr} S(k) \,. \tag{4.4}$$

This expression can now be evaluated for the propagator, which was obtained by the solution of the DSE. Evaluating the trace and performing a Wick rotation, the angular part of the integral can be carried out and we finally arrive at

$$\langle \overline{\psi}\psi \rangle_\mu = \; Z_2 Z_m \, \frac{d(\mathbf{R})}{4\pi^2} \int dk^2 \, \frac{k^2 \, Z(k^2) M(k^2)}{k^2 + M^2(k^2)} \,. \tag{4.5}$$

The dimension of the representation $d(\mathbf{R})$ enters due to the trace over the color space.
The integrand in the above equation vanishes sufficiently fast for large momenta, so that the integral is finite. An illustration of this can be seen in Fig. 4.2, where a double logarithmic display is chosen, in order to highlight the $1/k^2$ behavior for large momenta. Besides, it is made evident that the dominant contribution to the condensate originates from the small momentum regime. Though for the higher representations, the maximum of the integrand is slightly shifted towards larger momenta.

For the explicit calculation of Eq. (4.5), we extracted the product of renormalization constants $Z_2 Z_m$ from a massive solution. The renormalization group invariant condensate can then be calculated from its definition in Eq. (2.79). The results of our calculation are summarized in Table 4.1.
As can be seen, we found the value $\langle \overline{\psi}\psi \rangle_{\mathrm{inv}}^{1/3} = 0.049\,\mathrm{GeV}$ for the chiral condensate of a triplet fermion. This value is smaller than the expected order $\sim 0.2\,\mathrm{GeV}$ that is found also in other studies [51]. Presumably, the reason for this lower value is the applied approximation for the effective coupling α_{eff}. Within our study, it is based on the one-loop perturbative running coupling, whose IR pole position was calculated to be $\Lambda_{QCD} = 0.157\,\mathrm{GeV}$ (see Sec. 2.6.1). Studies, which explicitly fine tune their effective coupling in order to reproduce the low energy pion and kaon properties, typically apply larger scales of $\Lambda_{QCD} \simeq 0.250\,\mathrm{GeV}$

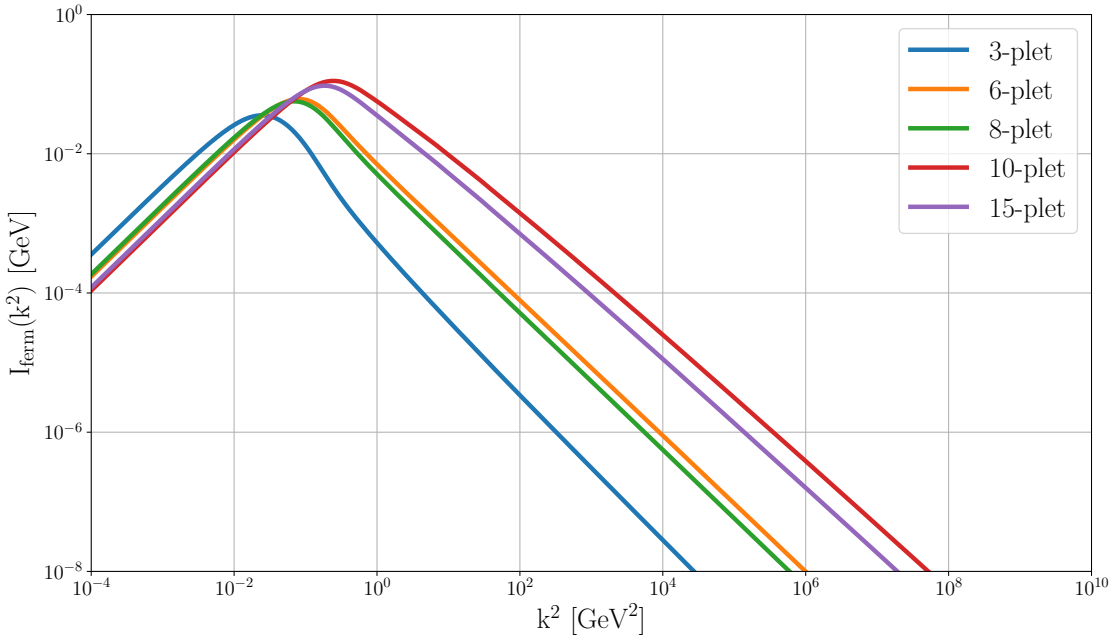

Figure 4.2 Behaviour of the integrand $I_{ferm}(k^2) \equiv k^2\, Z(k^2) M(k^2)/(k^2 + M^2(k^2))$ in the calculation of the chiral condensate $\langle\overline{\psi}\psi\rangle_\mu$ for different representations.

[50].

Nevertheless, the obtained result for the triplet is at the expected order of magnitude. Thus we assume, the relative behavior of different representations can be extracted from the acquired solution. We observe, that the value of the condensate generally increases for higher dimensional representations. Though, the result does not confirm the assumption of Lust et al. [10], who claimed that condensates of strongly interacting fermions in high dimensional representations could generate considerably larger scales than the triplet sector.

Rep (R)	$Z_2 Z_m$	d_m	$\langle\overline{\psi}\psi\rangle_\mu^{1/3}$	$\langle\overline{\psi}\psi\rangle_{inv}^{1/3}$
3	0.990	12/21	0.107 GeV	0.049 GeV
6	0.976	30/21	0.467 GeV	0.067 GeV
8	0.978	27/21	0.426 GeV	0.074 GeV
10	0.956	54/21	2.372 GeV	0.072 GeV
15	0.961	48/21	1.885 GeV	0.084 GeV

Table 4.1 Chiral condensate $\langle\overline{\psi}\psi\rangle_{inv}$ obtained from Eqs. (4.5) and (2.79) for fermions in different representations of the color gauge group.

Next, we will take the point of view of the operator product expansion and see, if the results obtained so far are consistent with this approach. As derived in Sec. 2.7, in the chiral limit, we expect the large momentum behavior of the dynamical mass to be

$$M(p^2) \overset{p\to\infty}{\simeq} \frac{4\pi^2 d_m}{d(\mathbf{R})} \langle\overline{\psi}\psi\rangle_{\text{inv}} \frac{1}{p^2} \left[\ln\left(p^2/\Lambda^2_{\text{QCD}}\right)\right]^{d_m-1} . \tag{4.6}$$

Using this ansatz, we can do a fit of Eq. (4.6) to the high momentum region of our numerical solution for $M(p^2)$. In order to do so, we used the expectation value of the condensate as a single fit parameter, with fixed values for d_m and $\Lambda_{QCD} = 0.157$ GeV and included a momentum region of $p^2 \geq 200\,\text{GeV}^2$ to be savely in the perturbative region.
The obtained results for the condensate are shown in Tab. 4.2 and demonstrate a good agreement to the values, which we calculated before (see Tab. 4.1). This confirms the consistency with the operator product expansion and simultaneously allows us to estimate the uncertainty of our calculation.
A graphical illustration of the resulting fit function is shown by the black dashed line in Fig. 4.3, being in good agreement to our numerical solution. Again, to explicitly highlight the momentum behavior, we selected a double logarithmic depiction in this plot, where the $1/p^2$ dependence appears as a straight line.
Meanwhile, the logarithm in Eq. (4.6) is of minor importance and does not contribute significantly in the large momentum region. Notice that if we include Λ_{QCD} as a second free fit parameter, the values for the condensates are almost unchanged.
On the other hand, we find a mild dependence of the results on the chosen fit interval. However, we see this method as a cross check of the preceding calculation and refrain from further evaluations of the fitting method.

Rep (R)	$\langle\overline{\psi}\psi\rangle_{\text{inv}}^{1/3}$
3	0.049 GeV
6	0.070 GeV
8	0.077 GeV
10	0.080 GeV
15	0.093 GeV

Table 4.2 Chiral condensate $\langle\overline{\psi}\psi\rangle_{\text{inv}}$ obtained from a fit of the operator product expansion in Eq. (4.6) to the numerical solution for the dynamical mass function $M(p^2)$.

To this end, we have described two methods to obtain the expectation value of the fermion condensate in the chiral limit. This is on the one hand a direct calculation from the integral in Eq. (4.5) and on the other hand from the asymptotic behavior, as described by the operator product expansion. We will now go on and consider the case, where fermions have explicit chiral symmetry breaking masses.

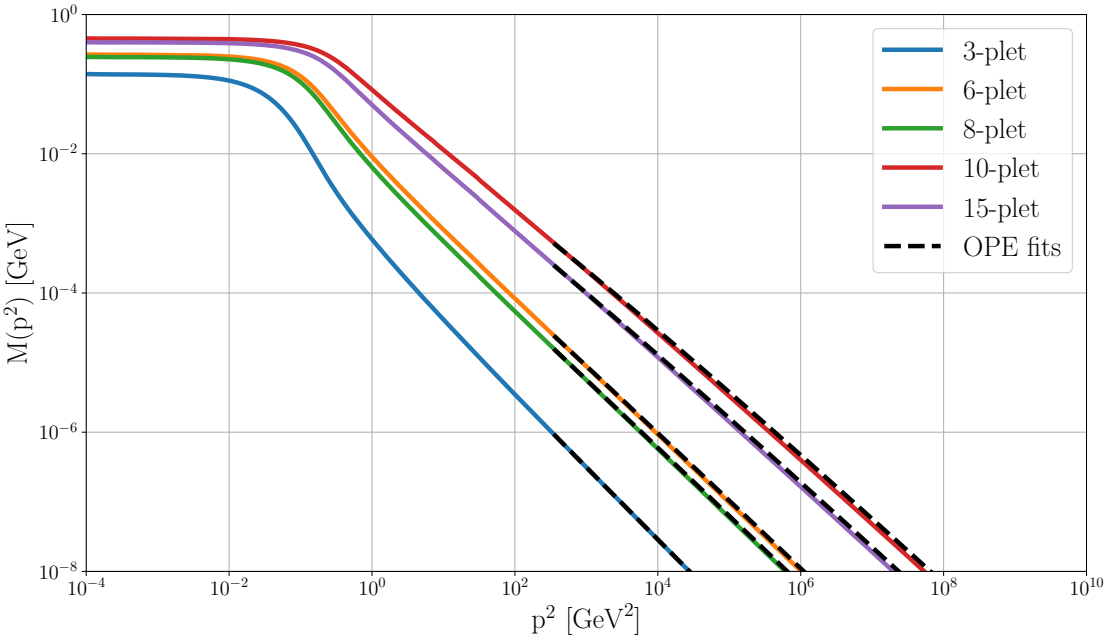

Figure 4.3 Fit of the operator product expansion to the large momentum behavior of the dynamical mass function $M(p^2)$. The obtained results for the fit parameter $\langle\overline{\psi}\psi\rangle_{\text{inv}}$ can be found in Tab. 4.2

4.2 Solution for Massive Fermions

Our analysis begins by considering a triplet fermion with an explicit mass $m \neq 0$, which experiences the one-loop Standard Model running, as illustrated in Fig. 3.1. We use this basic setting throughout this section, in order to illustrate the basic characteristics inherent to massive solutions. Also, we exemplify the extraction method of a lower bound for the condensate by a triplet fermion. The generalization to higher representations will then be subject of the next section.

Starting from this, the solution of the Dyson-Schwinger equation for different values of m can be found in complete analogy to the chiral case. The obtained results for the wave function renormalization and the mass function are shown in Fig. 4.4 for a selection of masses in a range between 1 MeV to 1 TeV. For comparison, the chiral limit is illustrated as well. The result shows, that the wave function renormalization is almost identical for all solutions in the UV, where the explicit mass is comparatively small to the considered momentum scale $m^2 \ll p^2$. Though in the IR, we see significant differences and the wave function renormalization takes lower values for smaller masses.
Concerning the mass function, our result does now include contributions from both the perturbative running of the explicit mass and a contribution from the non-perturbative

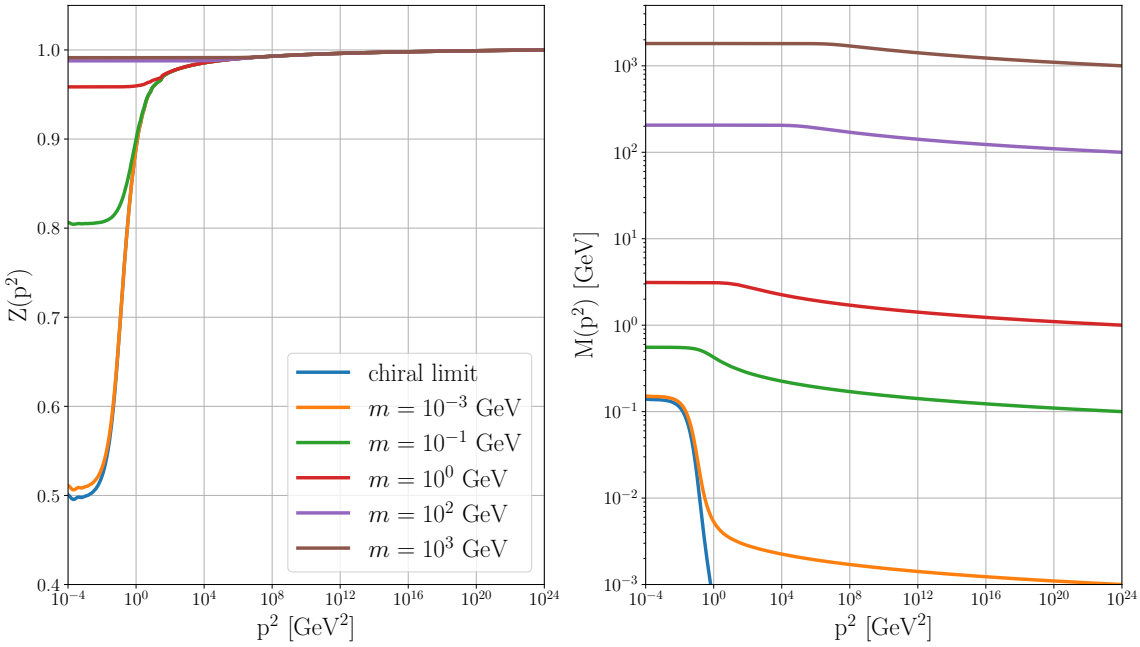

Figure 4.4 Wave function renormalization $Z(p^2)$ (left) and mass function $M(p^2)$ (right) for fermions in a triplet representation with different explicit masses m defined at the scale $\mu^2 = 10^{24}\,\mathrm{GeV}^2$. For comparison, the chiral limit $m = 0$ is depicted as well (blue line).

condensate. Besides, we should remember that the explicit masses are defined at the renormalization point $\mu^2 = 10^{24}\,\mathrm{GeV}^2$, where we applied the renormalization condition $M(p^2 = \mu^2) = m$ (see Sec. 2.5).

The solution for a light triplet fermion with $m = 10^{-3}$ GeV is almost identical to the chiral solution in the IR. For momenta $p^2 \gtrsim 10^{-2}\,\mathrm{GeV}^2$, we see a decrease of the mass function that follows the powers law $1/p^2$ and then passes over smoothly to a logarithmic running. This behavior illustrates the transition from the low momentum region, where the non-perturbative effects dominate the mass function, to the perturbative regime in the UV. The solutions for higher masses show in principle the same behavior. In the IR, the mass function is enhanced and drops off to lower values in the UV. Though, with growing mass, it is increasingly difficult to distinguish the perturbative and non-perturbative region.

We remark additionally, that while the mass function of the $m = 10^0$ GeV fermion starts to decrease at momenta $p^2 \gtrsim 10^1\,\mathrm{GeV}^2$, the solution with $m = 10^2$ GeV only falls off for values $p^2 \gtrsim 10^5\,\mathrm{GeV}^2$. Our first illustrative explanation for this observation is that the mass scale of the fermion, running in the loop of Fig. 2.4, suppresses contributions from relatively lower momenta. Therefore, the solution is insensitive to contributions from these lower scales. Nonetheless, this observation will be investigated further in the next section, where we will study the dominant contributions of the loop integral.

Finally, to provide a better view on the increase of the mass function for low momenta, we have a look at the quantity

$$\sigma(m) \equiv M(p^2 = 10^{-4}\,\mathrm{GeV}^2) - m\,, \tag{4.7}$$

which reflects the absolute enhancement of the mass function in the IR with respect to the explicit mass. The left plot of Fig. 4.5 shows, that $\sigma(m)$ increases with growing mass m. On the contrary, the relative enhancement $\sigma(m)/m$ (right plot) decreases for larger masses. Before we will turn to the question how the condensate can be extracted from the massive solution, we will try to understand the behavior of these solutions better. In order to do so, it is useful to take a look on the integrand of the loop integral, being part of the Dyson-Schwinger equation.

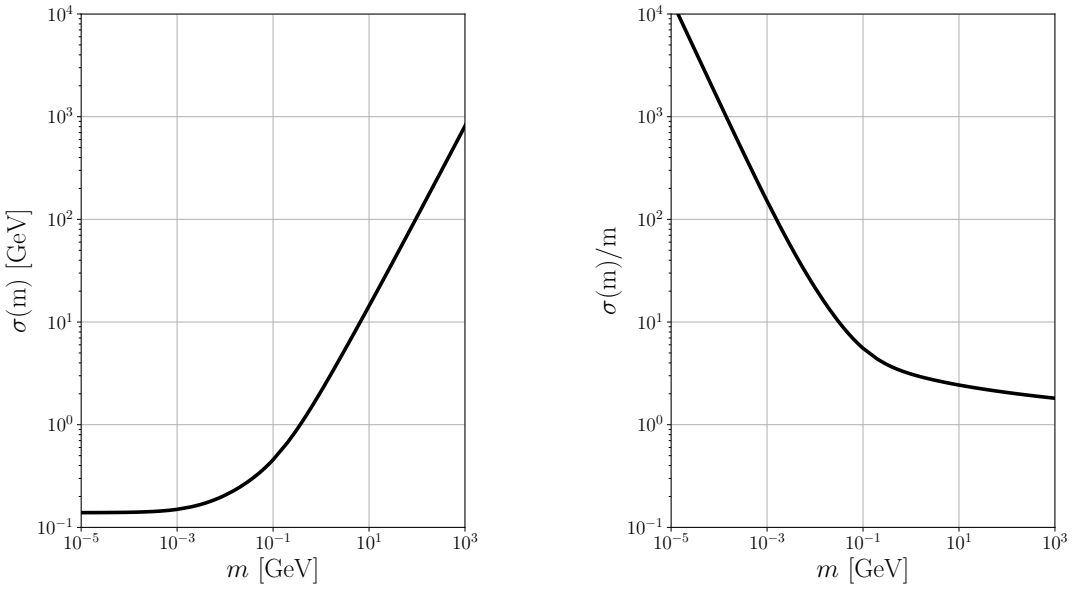

Figure 4.5 The absolute IR enhancement of the mass function $\sigma(m)$ defined in Eq. (4.7) (left) and the relative enhancement $\sigma(m)/m$ (right), obtained from the solution of the Dyson-Schwinger equation for a triplet fermion with different explicit masses m.

4.2.1 Analysis of the Loop Integral

The self-consistent solution of the DSE in Eq. (3.16) includes an integral over the loop momentum k that arises from the last Feynman diagram in Fig. 2.4. As a reminder, in Euclidean spherical coordinates it is given by

$$I(p^2) \equiv \int dk^2 \underbrace{\frac{k^2\, B(k^2)}{A^2(k^2)k^2 + B^2(k^2)}}_{I_{\text{ferm}}(k^2)} \underbrace{\int_0^\pi d\beta \sin^2(\beta) \frac{\alpha_{\text{eff}}\left((p-k)^2\right)}{(p-k)^2}}_{I_{\text{ang}}(p^2,k^2)}, \tag{4.8}$$

where p denotes the external momentum of the incoming fermion and the angle β is defined by $\cos(\beta) = p \cdot k/\sqrt{p^2 k^2}$. Since the first part of the above integrand originates from the fermion propagator, we will refer to this as fermionic part $I_{\text{ferm}}(k^2)$.

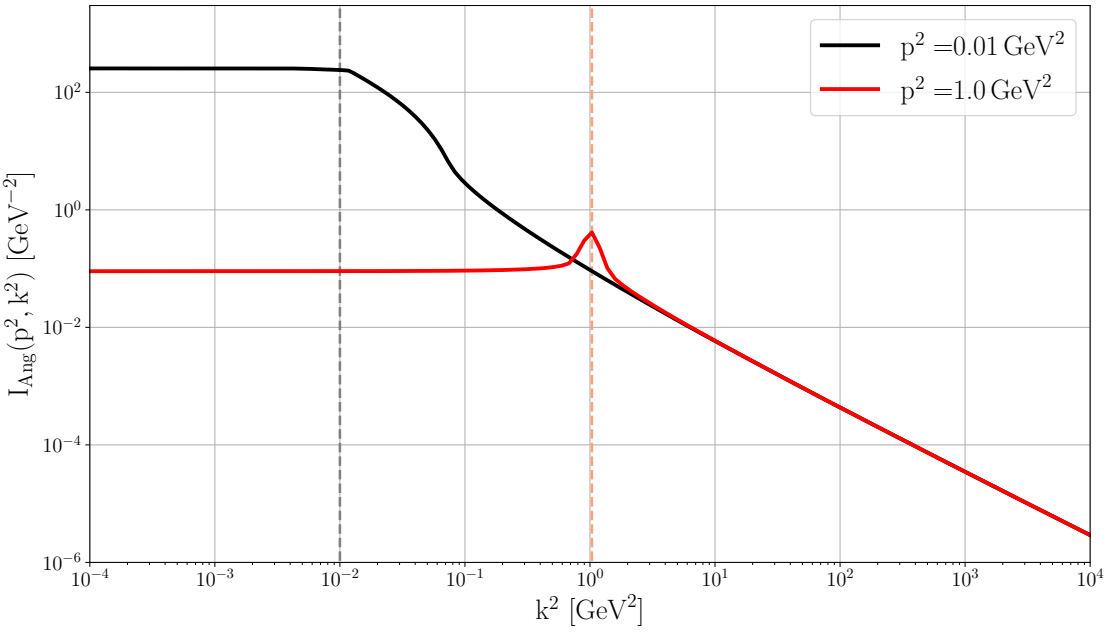

Figure 4.6 Behaviour of the angular integral $I_{\text{ang}}(p^2, k^2)$ defined in Eq. (4.8) as a function of the loop momentum k^2 for two fixed values of the external momentum p^2. The vertical dashed line indicates the position, where $k^2 = p^2$.

The second term of the integrand $I_{\text{ang}}(p^2, k^2)$, arising due to the vertices and the gluon propagator, includes the only non-trivial angular integration.
It is evident from the definition that the angular part of the integrand decouples except for its k dependence from the fermionic part, as in our current approximation we employ the same α_{eff} for all solutions. Thus in the following, we can consider the two parts by their own. Fig. 4.6 shows the result of the numerical calculation of $I_{\text{ang}}(p^2, k^2)$ as a function of k^2 for two fixed exemplary values of p^2. This general behavior can be understood, considering the following approximations

$$\int_0^\pi d\beta \sin^2(\beta) \frac{\alpha_{\text{eff}}((p-k)^2)}{(p-k)^2} \approx \begin{cases} \frac{\pi}{2} \frac{\alpha_{\text{eff}}(p^2)}{p^2}, & p^2 > k^2 \\ \\ \frac{\pi}{2} \frac{\alpha_{\text{eff}}(k^2)}{k^2}, & p^2 < k^2, \end{cases} \tag{4.9}$$

where the integration over the angle β became trivial. Thus, we expect a constant behavior in the region $p^2 > k^2$ (left side of the vertical dashed line) and a decrease, dominated by $1/k^2$, for the region $p^2 < k^2$ (right side of the vertical dashed line). The largest contribution to the angular integral arises when the four-vectors p and k are identical, i.e. for

$$p^2 = k^2 \qquad \text{and} \qquad z = \cos(\beta) = 1\,. \tag{4.10}$$

Though, as our α_{eff} is chosen finite also in the IR, the integral is convergent. Summarising, the angular part of the integrand receives the largest contributions from the region $k^2 \leq p^2$. We will continue with the second part of the integrand $I_{\text{ferm}}(k^2)$. Fig. 4.7 shows its behavior for different explicit masses. What we see, is a suppression of this part of the integrand for momenta $k^2 < m^2$, while the dominant contributions come from the region $k^2 > m^2$. In contrast, the chiral case obtains the largest contributions from the IR at around $10^{-2}\,\text{GeV}^2$ and afterwards decreases immediately. This result can also be understood from the formula itself. $I_{\text{ferm}}(k^2)$ can be rewritten in terms of the wave function renormalization and the mass function as

$$I_{\text{ferm}}(k^2) = \frac{k^2\, B(k^2)}{A^2(k^2)k^2 + B^2(k^2)} = \frac{k^2\, Z(k^2)\, M(k^2)}{k^2 + M^2(k^2)}\,. \tag{4.11}$$

From the right plot of Fig. 4.5 it can be seen that for large m, the mass function is dominated by the contribution of the explicit mass. Thus, we can use the rough approximation $M(p^2) \approx m$, which yields

$$\frac{k^2\, Z(k^2)\, M(k^2)}{k^2 + M^2(k^2)} \approx \frac{k^2\, m}{k^2 + m^2}\,, \tag{4.12}$$

using also the observation that $Z(p^2) \approx 1$ for large masses. The resulting equation gives a good approximation of the general behavior found in Fig. 4.7.

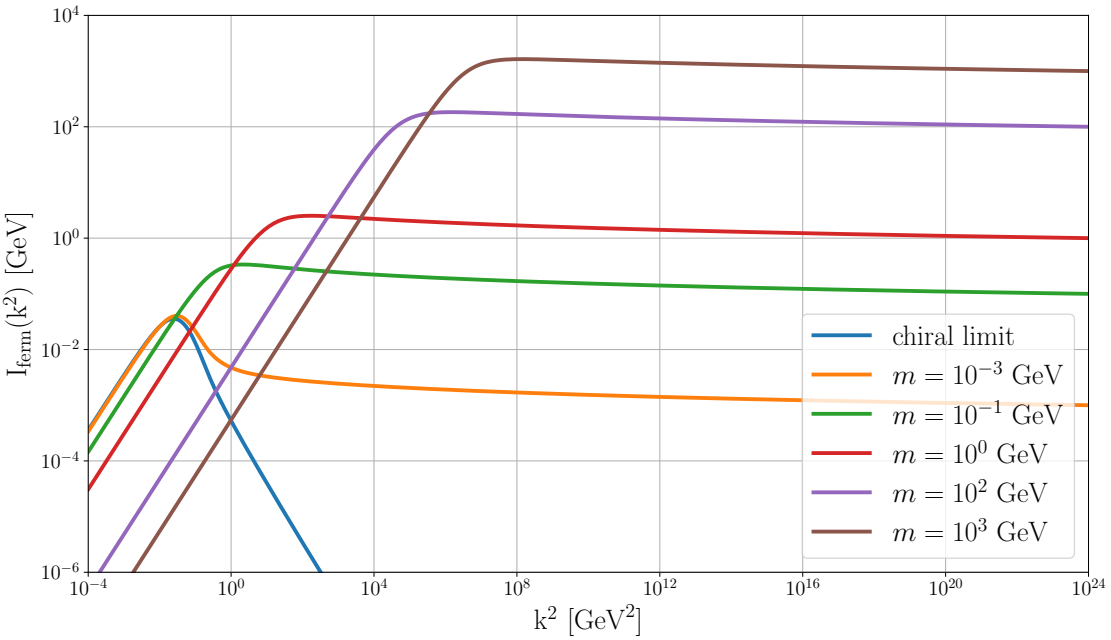

Figure 4.7 Behaviour of the fermionic part of the integrand $I_{\text{ferm}}(k^2)$ defined in Eq. (4.8) for different values of m and the chiral limit.

It is clear that the full integrand consists of the product of the two parts $I_{\rm ferm}(k^2)$ and $I_{\rm ang}(p^2,k^2)$. However, since the angular part of the integrand is common for all masses, we can conclude the following relative behavior. For small momenta, the contributions to the integrand are the more suppressed, the higher the explicit mass. Contrary in the UV, the larger the mass, the higher the contributions to the integrand. This verifies also our initial observation, that the mass function is insensitive to contributions from momenta lower than m.
Finally, we want to say a little more on the term $I_{\rm ferm}(k^2)$ on its own. As seen in Sec. 4.1.1, this integrand also appears in the calculation of the chiral condensate in Eq. (4.5).
If we would apply this equation naively for the massive case as well, we could estimate the integral to be

$$\begin{aligned}\int \frac{d^4k}{(2\pi)^2}\mathrm{Tr}_D S(k) &= \frac{1}{4\pi^2}\int dk^2 \frac{k^2\, Z(k^2)\, M(k^2)}{k^2+M^2(k^2)} \\ &\sim \int dk^2 \frac{k^2\, m}{k^2+m^2} \\ &\sim m\Lambda^2 + m^3 \ln\left(1+\frac{\Lambda^2}{m^2}\right).\end{aligned} \tag{4.13}$$

Here the UV cut-off Λ is introduced in the last line, to explicitly indicate the emerging quadratic and logarithmic divergences due to the explicit mass term.
This small calculation should only clarify that the formula in Eq. (4.5) cannot be applied to calculate the condensate of a massive fermion. In doing so, one would include divergent contributions from the explicit mass that are not connected to non-perturbative effects.
Hence, the question of the next section will be how one can consistently separate the non-perturbative contributions to the mass function from the perturbative ones.

4.2.2 Extraction of the Condensate

Apparently, the operator product expansion provides a good starting point for our aim to separate the contribution of the condensate from the mass function. This is because it already includes the different behavior of the two terms connected to explicit and dynamical chiral symmetry breaking. As a reminder, we quote here the result of the derivation in Sec. 2.7 for the case of a massive fermion:

$$M(p^2) \overset{p\to\infty}{\simeq} m\left[\frac{\ln\left(\mu^2/\Lambda^2_{QCD}\right)}{\ln\left(p^2/\Lambda^2_{QCD}\right)}\right]^{d_m} + \frac{4\pi^2 d_m}{d(\mathbf{R})}\frac{\langle\overline{\psi}\psi\rangle_{\rm inv}}{p^2}\left[\ln\left(\frac{p^2}{\Lambda^2_{\rm QCD}}\right)\right]^{d_m-1} + \ldots . \tag{4.14}$$

Note, that this expansion includes only the two lowest dimensional operators and the Wilson coefficients are calculated from the one-loop renormalization group equations.
In the chiral limit we have seen that the operator product expansion provides an excellent

tool to obtain the condensate, by fitting the high momentum behavior of the mass function. In continuing with the massive case, one could hope that this procedure might also work including the explicit mass term. However, as it turns out, this is a delicate task. Already for small masses, we see an extreme dependence of the result on the selected fit region and for larger masses it is almost impossible to capture the rapidly decreasing non-perturbative contribution in the presence of the dominating explicit mass term.
There are attempts to define an ambiguity free fit algorithm from the existence of unphysical negative solutions to the Dyson-Schwinger equation [52, 53]. However these are only successful in a small mass range.
This is the reason why we propose an alternative method to extract the condensate, motivated by a definition, which is commonly used in lattice calculations [51, 54, 55].
Starting point is the observation, that to the given order, the operator product expansion is linear in the explicit mass. Hence, if we consider the ratio $M(p^2)/m$, the perturbative part of the operator product expansion is the same for every solution, and it is possible to get rid of this term, by subtracting two distinct solutions from each other. This is the principle idea behind our method.
In a mathematically rigorous way, this can be implemented in form of derivatives with respect to m. Thus, we promote $M(p^2)$ to be not only a function of momentum, but also of mass $M(p^2) \to M(p^2, m)$. Considering Eq. (4.14), this manifests itself not only by an explicit dependence, but also by a dependence of the condensate $\langle\overline{\psi}\psi\rangle_{\text{inv}} \to \langle\overline{\psi}\psi\rangle_{\text{inv}}(m)$, which we assume in the following. Ultimately, it is the function $\langle\overline{\psi}\psi\rangle_{\text{inv}}(m)$ we want to obtain.
Hereafter, the derivative of some general function F with respect to m will be indicated by a prime $\frac{d}{dm}F(m) \equiv F'(m)$. With this at hand, we define the quantity

$$\begin{aligned} \Delta_{\text{M}}(p^2, m) &\equiv M(p^2, m) - m \cdot M'(p^2, m) \\ &\overset{p\to\infty}{\simeq} C(p^2, m) - m \cdot C'(p^2, m)\,, \end{aligned} \tag{4.15}$$

where the function $C(p^2, m)$ is given by the non-perturbative contribution to the operator product expansion

$$C(p^2, m) \equiv \frac{4\pi^2 d_m}{d(\mathbf{R})} \frac{\langle\overline{\psi}\psi\rangle_{\text{inv}}(m)}{p^2} \left[\ln\left(\frac{p^2}{\Lambda^2_{QCD}}\right)\right]^{d_m - 1}\,, \tag{4.16}$$

and the second equality in Eq. (4.15) assumes the further terms of the expansion to be negligible. We highlight that the function $C(p^2, m)$ has the same momentum dependence as the derivative $C'(p^2, m)$.
For the numerical determination of $M'(p^2, m)$, we solved the Dyson-Schwinger equation for 90 different masses in a range between $m = 10^{-5}\,\text{GeV} - 10^3\text{GeV}$ and calculated the derivative from the difference quotient. Fig. 4.8 shows the momentum behavior of the resulting function $\Delta_{\text{M}}(p^2, m)$ for a selection of values m, in case of a triplet fermion. To have a comparison, the mass function $M(p^2)$ for the chiral limit (blue line) is plotted as well.

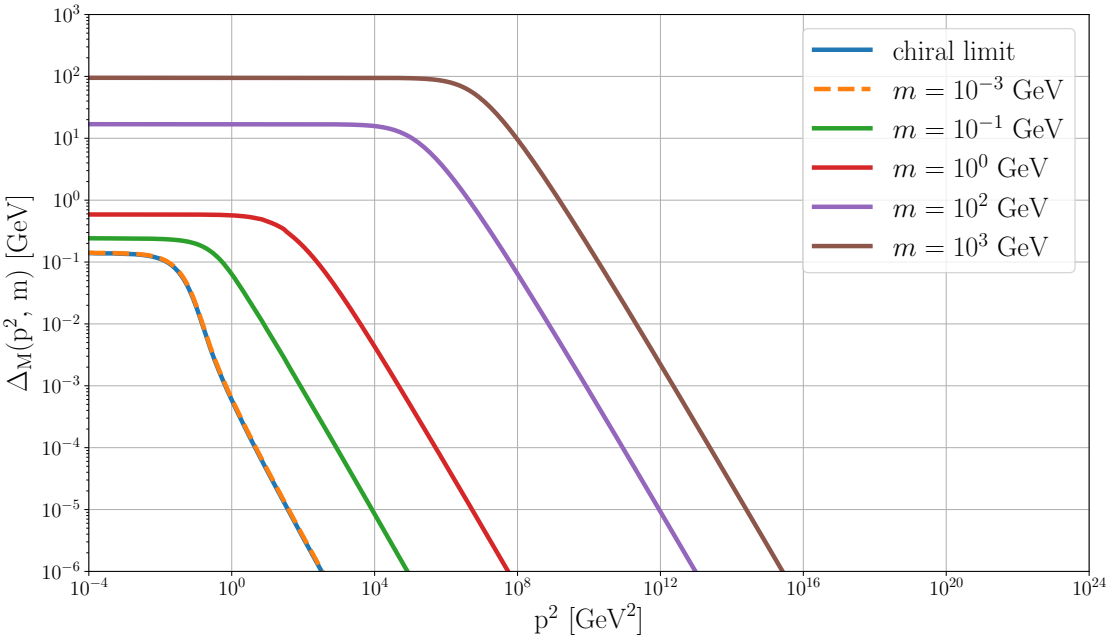

Figure 4.8 Behaviour of $\Delta_{\mathrm{M}}(p^2, m)$ defined in Eq. (4.15) as a function of p^2 for a triplet fermion with different values of m. For comparison, the mass function $M(p^2)$ of the chiral limit (blue line) is shown as well.

We see, that $\Delta_{\mathrm{M}}(p^2, m)$ has qualitatively the same momentum behavior as the chiral case, characterized by a rapid decrease in powers of $1/p^2$. The typical logarithmic tail, which is present for massive fermions in the mass function $M(p^2)$, has vanished. Based on that we assume that this procedure has successfully eliminated the first term of Eq. (4.14). Also, at first sight the large momentum dependence of $\Delta_{\mathrm{M}}(p^2, m)$ agrees with our expectation of that of the non-perturbative part of the operator product expansion $C(p^2, m)$.
In order to check whether the extracted function has truly the expected momentum behavior, we have a look at the quantity

$$\begin{aligned} \Delta_{\langle\bar{\psi}\psi\rangle}(p^2, m) \;&\equiv\; \Delta_{\mathrm{M}}(p^2, m) \cdot p^2 \frac{d(\mathbf{R})}{4\pi^2 d_m} \left[\ln\left(\frac{p^2}{\Lambda^2_{QCD}}\right)\right]^{-(d_m-1)} \\ &\overset{p\to\infty}{\simeq} \langle\bar{\psi}\psi\rangle_{\mathrm{inv}}(m) - m \cdot \langle\bar{\psi}\psi\rangle'_{\mathrm{inv}}(m)\,. \end{aligned} \tag{4.17}$$

On the basis of the operator product expansion, this should be independent of p^2 in the UV. The result for a selection of masses and the chiral case, is depicted in Fig. 4.9 . Note that we chose a different y-scale in each plot, in order to show only the relevant scale.
In case of the two smallest masses (second and third plot in Fig. 4.9) we see an almost constant behavior in the large momentum regime. This verifies that the approximation in the second line of Eq. (4.15) is reasonable and the two first terms of the operator product expansion are sufficient to describe the small mass range.
However, already for a mass of $m = 10^0$ GeV (fourth plot in Fig. 4.9), we see a mild

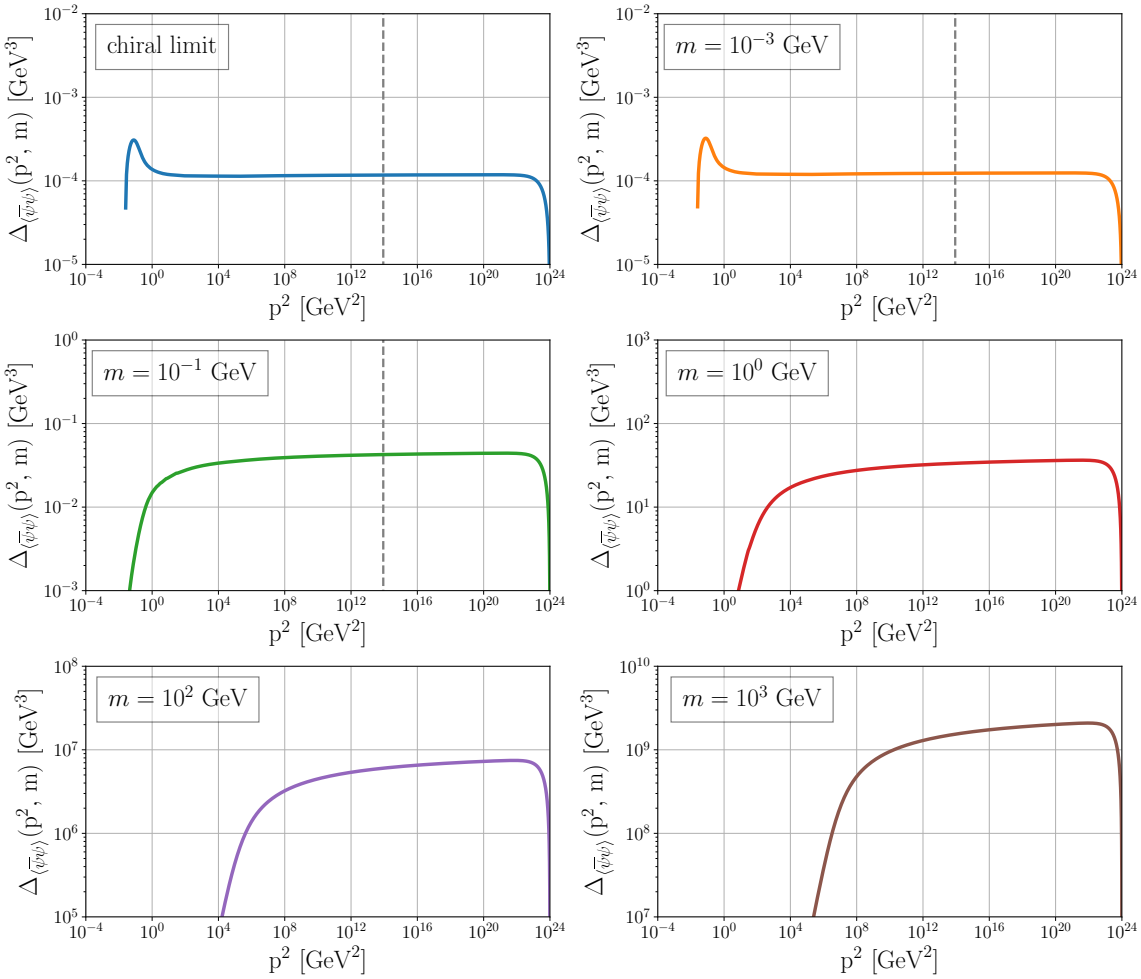

Figure 4.9 Behaviour of $\Delta_{\langle\overline{\psi}\psi\rangle}(p^2, m)$ defined in Eq. (4.17) as a function of p^2 for a triplet fermion with different values of m and the chiral limit. The vertical dashed line in the first three plots indicates, where we read off the constant UV value for masses up to $m \leq 10^{-1}$ GeV.

logarithmic running in the UV. An effect which strengthens with increasing mass. We believe that this is due to higher order corrections to the operator product expansion which are not negligible for large masses. Actually, our method eliminates terms linear in m. However, the example calculation in Eq. (4.13) has revealed also a cubic mass dependence that is inherent to the integration over the massive fermion propagator. Thus we believe that additional terms of the order $\sim \mathcal{O}(m^3/p^2)$ might contribute significantly to the operator product expansion for large m.

For this reason, we restrict the further analysis to masses up to $m \leq 10^{-1}$ GeV, where we verified from Fig. 4.9 that the next order terms are of minor importance.

We emphasize that this is also consistent with the observation that for approximately $m \gtrsim 10^{-1}$ GeV, the term m^3 becomes larger than the chiral condensate.

As a next step, we can read off the value $\left[\langle\overline{\psi}\psi\rangle_{\text{inv}}(m) - m \cdot \langle\overline{\psi}\psi\rangle'_{\text{inv}}(m)\right]$ from the UV behavior of the function $\Delta_{\langle\overline{\psi}\psi\rangle}(p^2, m)$. The dashed vertical line in the upper two plots of Fig. 4.9 indicates that we extracted this value at $p^2 = 10^{14}\,\text{GeV}^2$ for all solutions. This guarantees to be safely in the constant region.

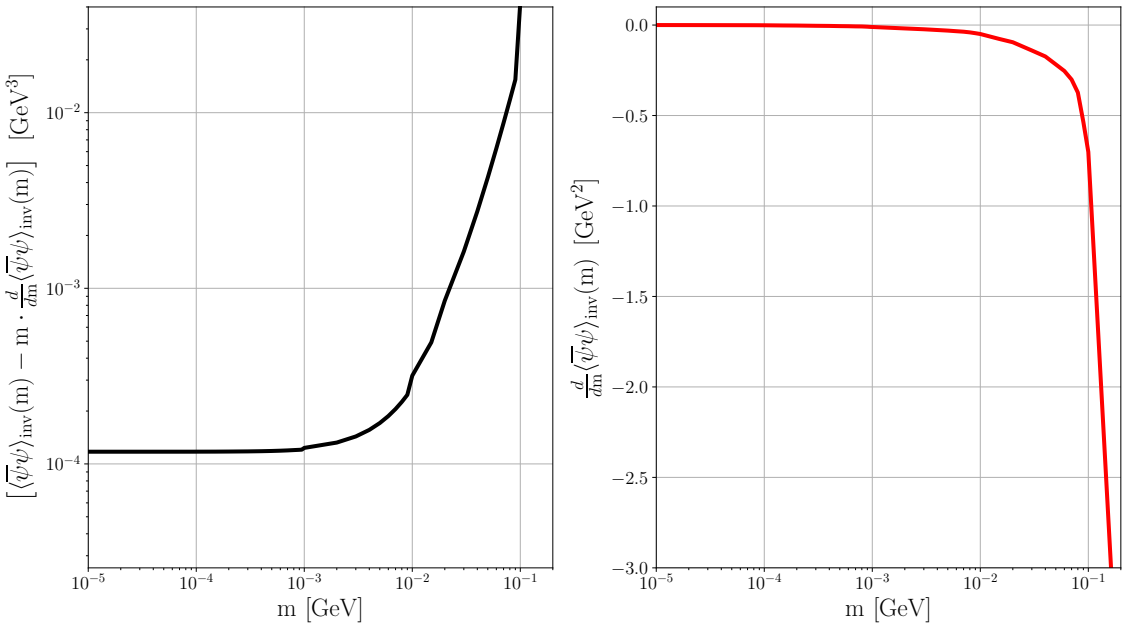

Figure 4.10 Extracted value $\left[\langle\overline{\psi}\psi\rangle_{\rm inv}(m) - m\cdot\langle\overline{\psi}\psi\rangle'_{\rm inv}(m)\right]$ as a function of m (left plot) and the behavior of $\langle\overline{\psi}\psi\rangle'_{\rm inv}(m)$ (right plot) which is only known up to the constant C_1. In this illustration, we chose the arbitrary value $C_1 = 0\,\mathrm{GeV}^2$.

As shown in the left plot of Fig. 4.10, the extracted value increases with m. Additionally we see, that in the limit $m \to 0$, the extracted value coincides with the chiral condensate of a triplet fermion, calculated in Sec. 4.1.1. This provides a consistency check for our method. Note that the minor kinks within the graph are simply an effect of the finite discretization in m.
In order to disentangle $\langle\overline{\psi}\psi\rangle_{\rm inv}(m)$ and its derivative, we differentiate one more time and arrive at an expression for the second derivative

$$-\frac{1}{m}\cdot\frac{d}{dm}\left[\langle\overline{\psi}\psi\rangle_{\rm inv}(m) - m\cdot\langle\overline{\psi}\psi\rangle'_{\rm inv}(m)\right] = \langle\overline{\psi}\psi\rangle''_{\rm inv}(m)\,, \tag{4.18}$$

This can subsequently be integrated to find

$$\int_0^m \langle\overline{\psi}\psi\rangle''_{\rm inv}(m)dm = \langle\overline{\psi}\psi\rangle'_{\rm inv}(m) - C_1\,. \tag{4.19}$$

Though, the derivative $\langle\overline{\psi}\psi\rangle'_{\rm inv}(m)$ is only known up to an integration constant C_1, which has the physical interpretation of the slope at mass zero, i.e.

$$C_1 = \langle\overline{\psi}\psi\rangle'_{\rm inv}(0)\,. \tag{4.20}$$

We show the extracted derivative $\langle\overline{\psi}\psi\rangle'_{\rm inv}(m)$ in the left plot of Fig. 4.10 for an exemplary value of $C_1 = 0\,\mathrm{GeV}^2$. Irrespective of this unknown constant, which only shifts the whole graph in y-direction, we observe a decrease in $\langle\overline{\psi}\psi\rangle'_{\rm inv}(m)$ for an increasing value of m.

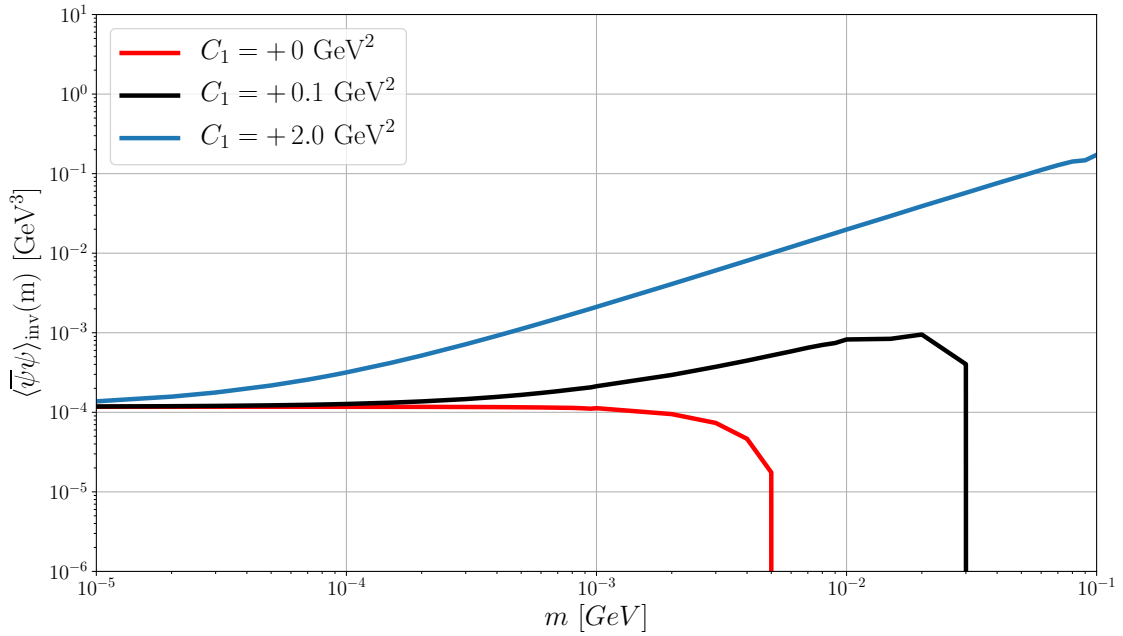

Figure 4.11 Condensate $\langle\overline{\psi}\psi\rangle_{\rm inv}(m)$ of a triplet fermion as a function of the explicit mass m, for a selection of different integration constants $C_1 = \langle\overline{\psi}\psi\rangle'_{\rm inv}(0)$. The self-consistency requirement of having no change in sign within the considered mass region demands a minimum value $C_1 = +2.0\,\mathrm{GeV}^2$ (blue line).

For now, we take C_1 as a new variable, being an artifact of our reparameterization of the non-perturbative contributions and see how our final result depends on this value. Fig. 4.11 shows the extracted value of the condensate $\langle\overline{\psi}\psi\rangle_{\rm inv}(m)$ for a choice of three different values of C_1. For $C_1 = 0\,\mathrm{GeV}^2$ (red line), we find an almost constant behavior for small masses which starts to drop off at around $m = 10^{-3}\,\mathrm{GeV}$ and becomes negative for masses higher than $m \geq 5 \cdot 10^{-3}\,\mathrm{GeV}$. The decrease of the value of the condensate is even faster, if we would choose C_1 to be negative. In contrast to that, a positive value of C_1 represents a positive slope at $m = 0$. Therefore, the decrease to negative values takes places at higher masses (black line in 4.11).

The fundamental question is, whether it is possible that the condensate changes from positive to negative values at some scale. In principle, there is no physical reason to assume that the condensate changes its sign. In doing so, an exceptional mass scale would be created, where the value of the condensate crosses zero. Hence, for self-consistency reasons we assume there should be no sign change within the mass range we believe our extraction method to be valid.

Under this assumption we can constrain the possible value of C_1. The minimum value, which fulfill this requirement up to masses $m \leq 10^{-1}\,\mathrm{GeV}$, is given by $C_1 = +2.0\,\mathrm{GeV}^2$. This should provide at least a lower bound for the value of $\langle\overline{\psi}\psi\rangle_{\rm inv}(m)$.

Under these assumptions, we see that the lower bound of the condensate increases with

growing mass. To give a concrete example, for a triplet fermion with $m = 10^{-3}\,\mathrm{GeV}$, we find a boundary value of

$$\langle\overline{\psi}\psi\rangle_{\mathrm{inv}}^{1/3} \geq 0.170\,\mathrm{GeV}\,. \tag{4.21}$$

This is roughly three times higher than what we found for the chiral condensate and agrees with values found in lattice simulations [51].
Finally we emphasize that in the case of $C_1 = +2\,\mathrm{GeV}^2$ the value of the condensate grows linearly in m. Hence, we expect the ratio $\langle\overline{\psi}\psi\rangle_{\mathrm{inv}}(m)/m$ to be convergent. This is in agreement with the relative enhancement of the complete dynamical mass function that was found in Fig. 4.5.

4.2.3 Generalization to Higher Representations

Now, that we have examined the massive solutions for triplet fermions, we want to turn to higher representations. The basic properties of these solutions are in principle similar to the fundamental representation. Therefore, we will not go through the whole extraction method in the same detail as before. Instead, we highlight the main intermediate steps and focus on the differences between the representations.
To provide insight in a more realistic model, we want to include the effect of the high colour fermion to the UV behavior of the running coupling. The calculation in Sec. 2.6.1 revealed that the asymptotic freedom of QCD is lost by the inclusion of an additional 10-plet fermion or a higher representation. For this reason, we restrict the following analysis to 6-plets and 8-plets [1]. Furthermore, since we are ultimately interested in a theory that includes a high color fermion with a mass of the order TeV, we use a running coupling, where we have included the contribution of a one TeV fermion for momenta $p^2 > (2m)^2$. The resulting UV behavior is illustrated in Fig. 2.5 .
We emphasize that this is an approximation. Ideally, one should include the contribution of each considered mass individually. For small masses this approximation leads to an error, as the contribution of a light additional 6-plet or 8-plet fermion[2] would shift the pole of the running coupling to lower values. However, if the mass threshold is high enough, the additional contribution only concerns the UV tail of the running coupling and our approximation has a minor effect.
Within the described approach, we show the wave function renormalization $Z(p^2)$ and the dynamical mass function $M(p^2)$ for a 6-plet and an 8-plet fermion with an exemplary mass of $m = 10^{-1}\,\mathrm{GeV}$ in Fig. 4.12. In order to provide a better comparison, we present the results for the 3-plet fermion from the last section as well.
We find that the mass function of the 6 -and 8-plet representation is significantly enhanced in the IR. This is nothing unexpected, as we already observed this behavior for the chiral

[1] The possible existence of multiple solutions to the DSE, due to a non-perturbative growing strong coupling in the UV would be an interesting investigation on its own.

[2] This is the case if the mass threshold is lower than Λ_{QCD}, i.e. in our calculation for $2m < \Lambda_{\mathrm{QCD}} = 0.157\,\mathrm{GeV}$ (see details in Sec. 2.6.1)

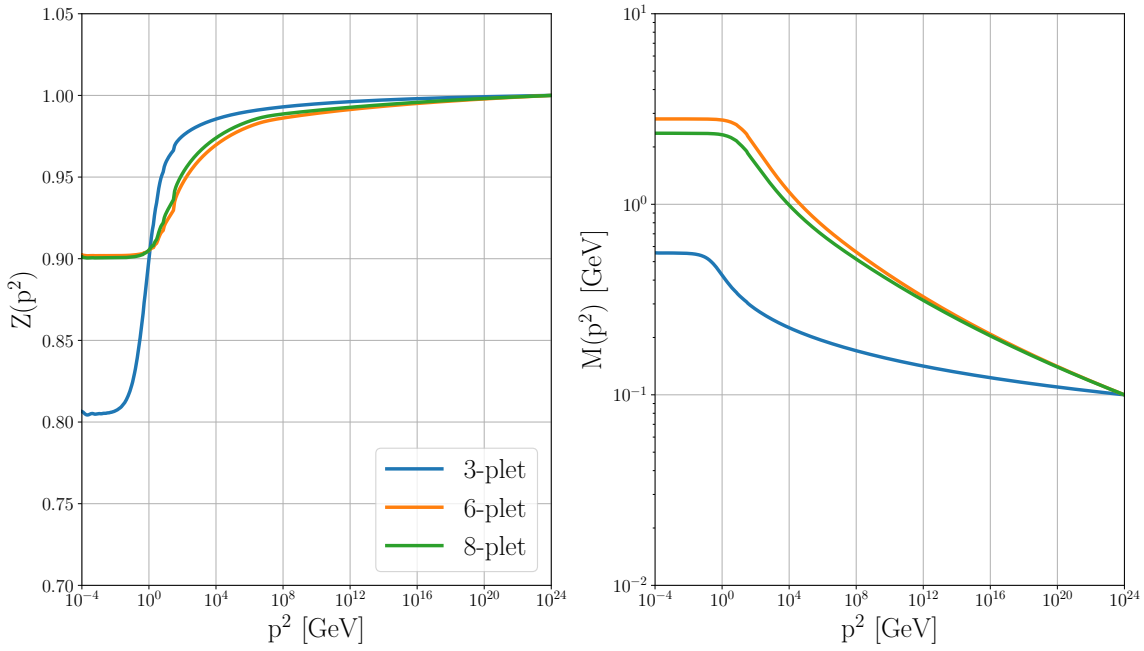

Figure 4.12 Wave function renormalization $Z(p^2)$ (left) and mass function $M(p^2)$ (right) for fermions in representations **3**, **6** and **8** with an explicit mass $m = 10^{-1}\,\mathrm{GeV}$.

case. Thereby, the mass function of the 6-plet exceeds that of the 8-plet, due to its higher Casimir constant (see Tab. 2.1).

Additionally, the mass functions shows a much stronger decrease for large momenta. This is owing to the anomalous dimension d_m, which is larger for higher representations (see Eq. (2.66)). Therefore, the perturbative running explicit mass, which dominates the UV behavior of the mass function, shows a steeper descent.

After we have applied our method to eliminate the first term of the operator product expansion in Eq. (4.14), the surviving non-perturbative contribution $\Delta_{\mathrm{M}}(p^2, m)$ shows a higher value for the 6 -and 8-plet representation than for the triplet (see left plot Fig. 4.13). Subsequently, we extract the assumed momentum behavior of the function $\Delta_{\mathrm{M}}(p^2, m)$ to arrive at $\Delta_{\langle\overline{\psi}\psi\rangle}(p^2, m)$, which is shown in the left plot of Fig. 4.13 for a fermion of mass $m = 10^{-1}\,\mathrm{GeV}$.

The plot illustrates, that also for higher representations, the quantity $\Delta_{\langle\overline{\psi}\psi\rangle}(p^2, m)$ is independent of p^2 for large momentum. Thus, we can read off the constant value $\left[\langle\overline{\psi}\psi\rangle_{\mathrm{inv}}(m) - m \cdot \langle\overline{\psi}\psi\rangle'_{\mathrm{inv}}(m)\right]$ from the plateau region.

Note that the interchanged ordering between the 6-plet and 8-plet representation stems from the fact, that the dimension $d(\mathbf{R})$ enters in $\Delta_{\langle\overline{\psi}\psi\rangle}(p^2, m)$. For masses higher than $10^{-1}\,\mathrm{GeV}$, our results indicate that the next order terms in the operator product expansion are necessary for a reliable description. Therefore, we proceed similar to the triplet case and extract a lower bound for the condensate, by constraining the unknown value of $C_1 = \langle\overline{\psi}\psi\rangle'_{\mathrm{inv}}(0)$ in a way that there is no change in sign up to $m \leq 10^{-1}\,\mathrm{GeV}$. In other words, we request the results to be self-consistent up to a certain mass scale.

For the 6-plet fermion we find a minimal value $C_1 = 25\,\mathrm{GeV}^2$ and for the 8-plet $C_1 =$

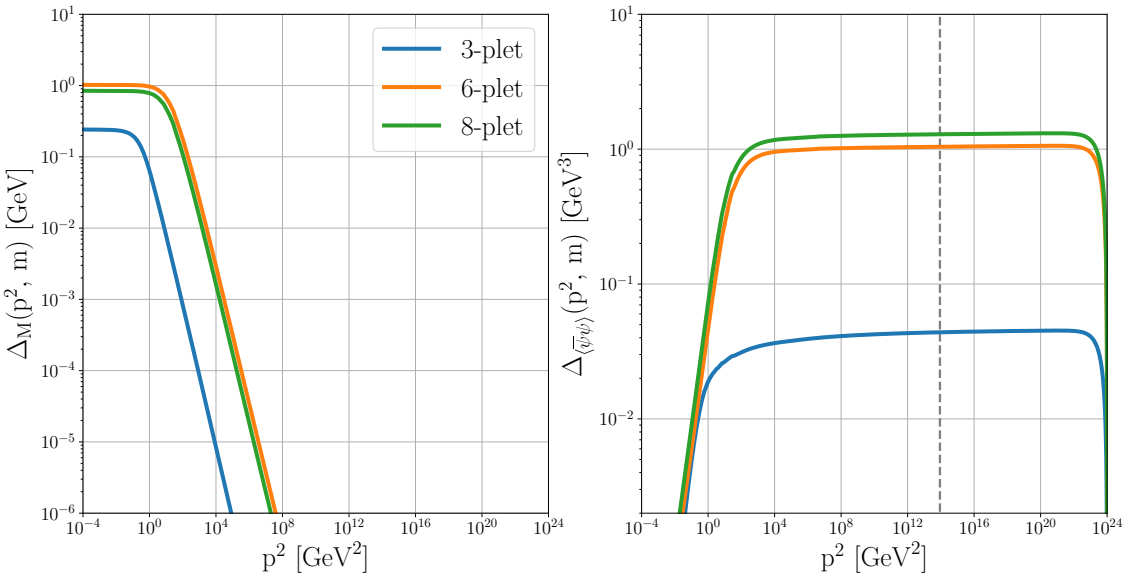

Figure 4.13 Momentum dependence of the functions $\Delta_M(p^2, m)$ (left) and $\Delta_{\langle\bar{\psi}\psi\rangle}(p^2, m)$ (right), defined in Eqs. 4.15 and 4.17, for fermions in representations **3**, **6** and **8** with an explicit mass $m = 10^{-1}$ GeV. The vertical dashed line in the right plot indicates, where we read off the momentum independent value $\left[\langle\bar{\psi}\psi\rangle_{\text{inv}}(m) - m \cdot \langle\bar{\psi}\psi\rangle'_{\text{inv}}(m)\right]$.

$35\,\text{GeV}^2$. The result of this approach is illustrated by the solid lines in Fig. 4.14, where we find a linear increase with mass for all representations. Furthermore, our procedure yields that the resulting lower bound is higher for the 6-plet and 8-plet representations as for the triplet.

We want to discuss now, whether this result allows conclusions for the higher mass range. Until now, we do not know if the occurrence of a sign change in the condensate is a feasible scenario or not. Nevertheless, starting from the fundamental assumption that this should not be the case, our analysis in the small mass regime has shown that it is always possible to find a minimal value C_1 for which there is no sign change up to a certain mass scale. If we assume that the general behaviour for masses larger than $m = 10^{-1}$ GeV does not drastically change, then it should in principle also be possible to find a minimal value C_1 which fulfills this requirement up to higher masses. In particular our analysis indicates that this would demand a larger value of C_1 which raise the lower bound for the condensate to higher values (see Fig. 4.11). On the basis of these assumptions we believe the linear extrapolation of the lower bound we found by requesting self-consistency up to $m = 10^{-1}$ GeV should in particular also be a lower bound for higher masses. An illustration of this extrapolation is shown by the dashed line in Fig. (4.14).

Nonetheless, we want to stress that this bases on the one hand on the assumption that there exits a minimal value C_1 for which there is no change in sign of the condensate up to the TeV scale and secondly that this value is equal or higher than that we found by requesting consistency up to $m = 10^{-1}$ GeV.

To answer whether these assumptions are correct, it would be necessary to extend our

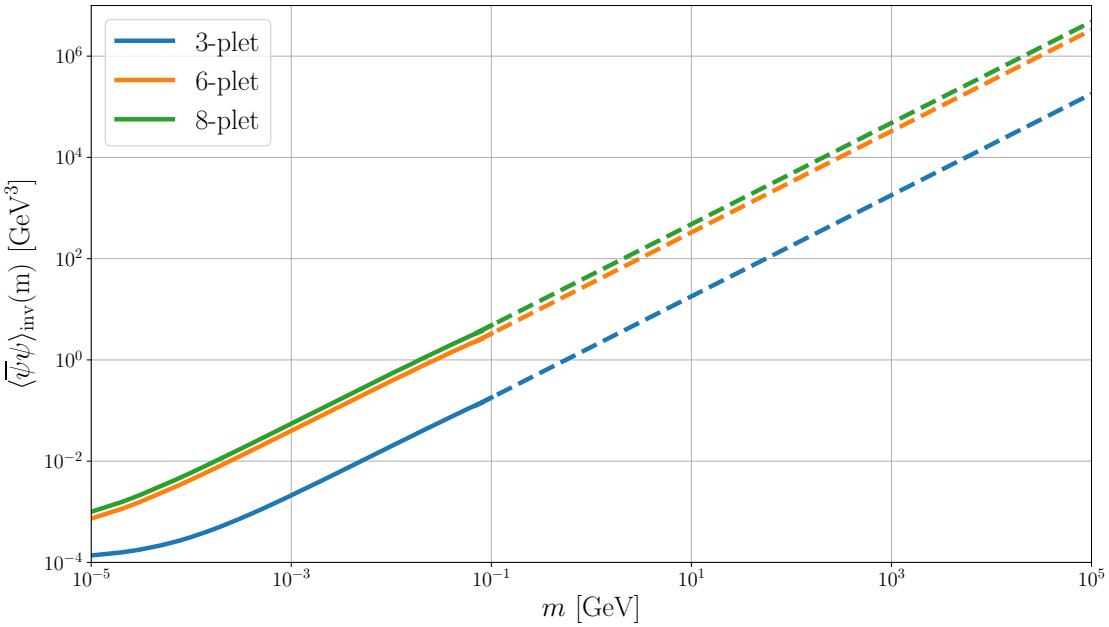

Figure 4.14 Lower bound for the condensate $\langle\overline{\psi}\psi\rangle_{\rm inv}(m)$ of massive fermions in representations **3**, **6** and **8** (solid lines), where the minimum value of the unknown constant $C_1 = \langle\overline{\psi}\psi\rangle'_{\rm inv}(0)$ is chosen for each representation such that there is no change in sign for $m \leq 10^{-1}$ GeV. The dashed lines indicates a linear extrapolation of the found behavior to higher masses.

extraction method of the non-perturbative part of the dynamical mass function to higher explicit masses by including the next order term of the operator product expansion. Then, we could examine what particular choice of C_1 would be necessary to guarantee that the condensate is positive up to larger masses. We note also that for the triplet case this result then needs to be cross checked not to be in conflict with the known condensates of the lightest quarks.

Nonetheless, under these assumption the extrapolation shown in Fig. 4.14 suggest that a 6-plet or 8-plet fermion with a mass of roughly around $\sim 10\,\mathrm{TeV}$ could have a condensate at the order of the electroweak scale

$$\langle\overline{\psi}\psi\rangle_{\rm inv}^{1/3} \gtrsim 100\,\mathrm{GeV}\,. \tag{4.22}$$

We will give a short overview in the next chapter how this scale could be transmitted to the Standard Model in order to induce a VEV of the Higgs boson.

Chapter 5

Outlook to the Model

In this chapter we will give a short outlook on the possible realization of a model that includes a fermion in a high color representation. With this we mainly intend to outline an approach how the scale of chiral symmetry breaking in the new fermion sector could be transmitted to the Standard Model.

In summary, the principle idea of our study is to introduce a vector-like fermion in a high representation of the color gauge group. Due to non-perturbative effects of the running coupling, the new fermion forms a condensate and therefore dynamically breaks chiral symmetry. The question is how the scale that is generated by the condensate can be transmitted to the Standard Model in order to induce EWSB. In the original proposal by Lüst, Papantonopoulos and Zoupanos, the high color fermion itself carries the charge of the electroweak gauge group [9, 10]. Hence, electroweak symmetry is directly broken by the condensate. Since nowadays the electroweak precision observables severely constrain new physics in the electroweak sector, we refrain from this approach. Instead, we propose an indirect scale transmission by a singlet scalar mediator S which couples to both the new fermion and the Standard Model Higgs boson ϕ. In more detail, this works as follows.
With the assigned charges given in Tab. 5.1, the high color fermion can be coupled to the scalar S by a Yukawa interaction. Then the Lagrangian of the vector-like fermion sector is given by

$$\mathcal{L}_{\mathrm{VLF}} = \overline{\psi}\left(i\not{D} - m - yS\right)\psi\,, \tag{5.1}$$

with the first two terms describing the dynamics and explicit mass of the fermion and the last term denoting the Yukawa interaction with the dimensionless coupling y.
We highlight that the high representation of the new fermion forbids a direct coupling to ordinary triplet quarks. Therefore, there are no further constraints from mixing with Standard Model particles at tree level.

Particle	$SU(3)_c$	$SU(2)_L$	$U(1)_Y$
ψ	$\mathbf{R}$	$\mathbf{1}$	0
S	$\mathbf{1}$	$\mathbf{1}$	0

Table 5.1 Representations of the newly added fermion ψ and scalar S under the Standard Model gauge group with $\mathbf{R} \in \{\mathbf{6}, \mathbf{8}\}$.

In our model, we assume classical scale invariance of the scalar sector and the explicit mass of the high color fermion constitutes the only emerging energy scale. Therefore, the scalar potential is given by

$$V(\phi, S) = \lambda_\phi (\phi^\dagger \phi)^2 + \frac{1}{4}\lambda_S S^4 - \frac{1}{2}\lambda_{\phi S} S^2 (\phi^\dagger \phi)\,, \tag{5.2}$$

with the quartic couplings λ_ϕ and λ_S and the scalar portal coupling $\lambda_{\phi S}$. We emphasize that classical scale invariance forbids explicit mass terms for S and ϕ which would in principle be allowed by gauge invariance under the Standard Model gauge group.
Next, the formation of the high color fermion condensate acts as a source term that introduces a scale to the potential in form of a tadpole term that is generated for S. In terms of a tree level effective potential, this can be written as

$$V_{\text{eff}}(\phi, S) = \lambda_\phi (\phi^\dagger \phi)^2 + \frac{1}{4}\lambda_S S^4 - \frac{1}{2}\lambda_{\phi S} S^2 (\phi^\dagger \phi) - y\langle\overline{\psi}\psi\rangle_{\text{inv}} S\,. \tag{5.3}$$

By this, the scalar S can acquire a VEV which is subsequently transmitted to the Higgs boson by the scalar portal term, thus triggering EWSB.
For the successful development of non-zero expectation values of both scalars, the potential must satisfies the stability condition $4\lambda_\phi \lambda_S > \lambda_{\phi S}^2$ and additionally $\lambda_\phi > 0$ and $\lambda_S > 0$. Then using the notation in unitary gauge for ϕ, the scalar fields can be expanded around their minima

$$\phi(x) = \frac{1}{\sqrt{2}} \begin{pmatrix} 0 \\ v + h(x) \end{pmatrix}\,, \qquad S(x) = w + s(x)\,, \tag{5.4}$$

where v and w denote the VEV's of the two scalars. From minimization of Eq. (5.3) we find that the ratio of their VEV's is given by

$$\frac{v^2}{w^2} = \frac{\lambda_{\phi S}}{2\lambda_\phi}\,, \tag{5.5}$$

with

$$w^2 = \left(\frac{4y\lambda_\phi \langle\overline{\psi}\psi\rangle_{\text{inv}}}{4\lambda_\phi \lambda_S - \lambda_{\phi S}^2} \right)^{\frac{2}{3}}\,, \tag{5.6}$$

yielding a Higgs VEV of

$$v^2 = \frac{\lambda_{\phi S}}{2\lambda_\phi} \left(\frac{4y\lambda_\phi \langle\overline{\psi}\psi\rangle_{\text{inv}}}{4\lambda_\phi \lambda_S - \lambda_{\phi S}^2} \right)^{\frac{2}{3}}\,. \tag{5.7}$$

Our study in the previous chapter suggests that the condensate of a 6-plet or 8-plet fermion with a mass of $\sim 10\,\mathrm{TeV}$ could be at least of the scale $\langle\overline{\psi}\psi\rangle_{\mathrm{inv}}^{1/3} \gtrsim 100\,\mathrm{GeV}$. If we use the lower bound, the exemplary selection of couplings

$$y = 1\,, \qquad \lambda_\phi = 0.18\,, \qquad \lambda_S = 0.02\,, \qquad \lambda_{\phi S} = 0.09\,, \tag{5.8}$$

leads to the VEV's of the two scalars

$$\begin{aligned} v &= 243\,\mathrm{GeV}\,, \\ w &= 485\,\mathrm{GeV}\,. \end{aligned} \tag{5.9}$$

This example calculation demonstrates that with a suitable choice of parameters we can induce a VEV of the Higgs boson that is at the correct order to trigger EWSB in the Standard Model. In particular from Eq. (5.7) we realize that by adjusting the couplings of the scalar potential, the scale of the VEV's can be larger than the original scale of the condensate. Although this requires an explicit fine tuning of the parameters.
To close this Chapter, we stress that this should only provide an outlook on the possible scale transmission. A detailed study of the parameter space and the according scalar mass spectrum is beyond the scope of this thesis and will be left for future work.

Chapter 6

Summary and Conclusion

From a theoretical point of view, the origin of the electroweak scale and its smallness compared to the Planck scale is one of the intriguing puzzles of the Standard Model. In this thesis we studied a mechanism which attempts to provide a dynamical explanation for the generation of the electroweak scale. Namely, we investigated whether a vector-like fermion in a high representation of the color gauge group can form a chiral symmetry breaking condensate of the order of the electroweak scale which indirectly triggers EWSB.
The main part of this thesis was dedicated to explore the impact of the representation on the condensate and to answer the question in what sense a vector-like explicit mass of the fermion influences dynamical chiral symmetry breaking.
To address these questions, we solved the Dyson-Schwinger equation for the fermion propagator. We used a truncation scheme where the full fermion-gluon vertex was replaced by the bare one (rainbow-approximation) and applied a phenomenologically motivated effective running coupling to incorporate the non-perturbative effects of the unknown dressed gluon propagator (see Chapter 3).
We found that if the applied effective running coupling provides sufficient integrated strength in the IR, there are two distinct solutions to the Dyson-Schwinger equation in the chiral limit. Precisely, there is one chiral symmetry preserving solution, where the mass is exactly zero, and one solution with a dynamically generated mass breaking chiral symmetry.
This manifests that dynamical chiral symmetry breaking is present within the applied truncation.
Our analysis started by considering the simplified model of a high color fermion in the chiral limit that experiences the one-loop perturbative running coupling of the Standard Model. From the chiral symmetry breaking solution of the DSE, we calculated the expectation value of the condensate up to the 15-plet representation. For this purpose, we used two different methods. The first one bases on the formal definition of the chiral condensate in Eq. (4.1) and the second method uses a fit of the OPE to the large momentum behavior of our numerical solution. The obtained results are summarized in Tabs. 4.1 and 4.2 and show a good agreement that validated the consistency of the two approaches. For a chiral triplet condensate we found $\langle\overline{\psi}\psi\rangle_{\text{inv}}^{1/3} = 0.049\,\text{GeV}$ which is lower than the expected order $\sim 0.2\,\text{GeV}$ [51]. We believe this to be a consequence of our applied approximation

for the effective running coupling providing too little integrated strength in the IR (see Sec. 4.1.1). Within our approximation, we found a generally increasing condensate for higher representations. For example, our analysis yielded $\langle\overline{\psi}\psi\rangle_{\text{inv}}^{1/3} = 0.067\,\text{GeV}$ for a 6-plet fermion which is around 30% higher than the triplet condensate. Nevertheless, we did not observe the generation of significantly larger scales solely due to the higher representation as suggested by Lüst et al. [9, 10].

Next, we considered fermions with an explicit symmetry breaking mass. In this case, the dynamical mass function shows a qualitatively different behavior since it includes not only non-perturbative contributions connected to dynamical chiral symmetry breaking but also the perturbatively running explicit mass (see Fig. 4.4). We proposed a method to extract the non-perturbative contributions under usage of the first two terms of the OPE (see Sec. 4.2.2). From our studies, we believe this approach to be reliable for explicit masses up to approximately $m = 10^{-1}\,\text{GeV}$ as higher order corrections to the OPE become significant for larger masses. Remnant of our extraction method is the appearance of the variable $C_1 \equiv \frac{d}{dm}\langle\overline{\psi}\psi\rangle_{\text{inv}}(m = 0)$ that is the slope of the condensate at zero mass. We considered this unknown quantity as a new parameter and calculated the condensate for different C_1 (see Fig. 4.11). Our study revealed that if C_1 is chosen too small, the expectation value of the condensate changes from positive to negative values within the considered mass range. Since there is no physical reason to assume that this should be the case, we constrained the parameter space and found the minimum value C_1 which fulfills the requirement of having no change in sign up to the mass scale we believe our extraction method to be valid. This yielded a lower bound for the condensate that increases linearly with the explicit mass.

Our analysis in the small mass regime showed that it is always possible to find a minimum value for C_1 such that the expectation value of the condensate does not change its sign up to a certain mass scale. As we do not expect a fundamental change in the behavior for larger masses, we assumed that this should also be the case for the higher mass range. Our study indicated that this requires a larger value C_1 which lifts the lower bound for the condensate. Hence, in a first approximation the linear extrapolation of the lower bound we found by requesting consistency up to $m = 10^{-1}\,\text{GeV}$ should in particular also be a lower bound for higher masses.

Basing on the described assumptions we carried out our analysis for massive 6-plet and 8-plet representations as these do not destroy the asymptotic freedom of QCD by their additional contribution to the running coupling constant. We compared our results to the triplet case and found that the lower bound for the condensate is higher for 6-plet and 8-plet representations (see Fig. 4.14). Furthermore, our study suggests that a 6-plet or 8-plet fermion with an explicit mass of $\sim 10\,\text{TeV}$ could have a condensate of the order of the electroweak scale $\langle\overline{\psi}\psi\rangle_{\text{inv}}^{1/3} \gtrsim 100\,\text{GeV}$. With this result we gave an outlook for a possible scale transmissions to the Standard Model by a singlet scalar mediator that induces a VEV for the Higgs boson and thereby indirectly causes EWSB (see Chap. 5).

These initial results motivate to study the suggested mechanism in more detail. For this purpose, our method to extract the non-perturbative contribution to the dynamical mass

function constitutes a useful starting point that can be extended to include the next order term of the OPE. This would make a further analysis of the high mass range to an interesting work for future studies.

Appendix A

Conventions

A.1 Units

Throughout the whole thesis, we use natural units, i.e.

$$\hbar = c = 1\,. \tag{A.1}$$

A.2 Dirac Algebra

The chosen convention for the metric $g^{\mu\nu}$ is

$$g^{\mu\nu} = \mathrm{diag}(1,\,-1,\,-1,\,-1)\,. \tag{A.2}$$

The Dirac matrices fulfill the anti-commutation relation

$$\{\gamma^\mu, \gamma^\nu\} = 2g^{\mu\nu}\,. \tag{A.3}$$

During the calculations carried out within this thesis, the following identities have frequently been used:

$$g^{\mu\nu}g_{\mu\nu} = 4\,, \tag{A.4}$$

$$\gamma_\mu g^{\mu\nu}\gamma_\nu = \gamma^\nu\gamma_\nu = 4\,, \tag{A.5}$$

$$\gamma^\mu\gamma^\nu\gamma_\mu = -2\gamma^\nu\,. \tag{A.6}$$

Additionally, there are useful trace identities

$$\mathrm{Tr}_D\left[\gamma^\mu\right] = \mathrm{Tr}_D\left[\gamma^\mu\gamma^\nu\gamma^\sigma\right] = \mathrm{Tr}_D\left[\text{uneven number of } \gamma\text{−matrices }\right] = 0 \tag{A.7}$$

$$\mathrm{Tr}_D\left[\gamma^\mu\gamma^\nu\right] = 4g^{\mu\nu}\,. \tag{A.8}$$

Einstein summation convention is used throughout the whole thesis. Furthermore, the Dirac slash notation is used, defined by

$$A_\mu \gamma^\mu \equiv \not{A} \,, \tag{A.9}$$

where A_μ is some covariant vector. In analogy, we define

$$\gamma^\mu D_\mu \equiv \not{D} \,. \tag{A.10}$$

A.3 Fundamental Representation of $SU(2)$ and $SU(3)$

Commonly, the generators of the fundamental representation of $SU(2)$ are expressed in terms of the Pauli matrices which are given by

$$\sigma^1 = \begin{pmatrix} 0 & 1 \\ 1 & 0 \end{pmatrix} \,, \quad \sigma^2 = \begin{pmatrix} 0 & -i \\ i & 0 \end{pmatrix} \,, \quad \sigma^3 = \begin{pmatrix} 1 & 0 \\ 0 & -1 \end{pmatrix} \,, \tag{A.11}$$

and fulfill the relation

$$\sigma^i \sigma^j = \delta^{ij} \mathbb{1}_{2\times 2} + i\epsilon^{ijk} \sigma^k \,. \tag{A.12}$$

In case of the group $SU(3)$, a description of the generators of the fundamental representation is provided by the eight Gell-Mann matrices

$$\begin{aligned} \lambda^i &= \begin{pmatrix} \sigma^i & & 0 \\ & & 0 \\ 0 & 0 & 0 \end{pmatrix} \,, \quad \lambda^4 = \begin{pmatrix} 0 & 0 & 1 \\ 0 & 0 & 0 \\ 1 & 0 & 0 \end{pmatrix} \,, \quad \lambda^5 = \begin{pmatrix} 0 & 0 & -i \\ 0 & 0 & 0 \\ i & 0 & 0 \end{pmatrix} \,, \\ \lambda^6 &= \begin{pmatrix} 0 & 0 & 0 \\ 0 & 0 & 1 \\ 0 & 1 & 0 \end{pmatrix} \,, \quad \lambda^7 = \begin{pmatrix} 0 & 0 & 0 \\ 0 & 0 & -i \\ 0 & i & 0 \end{pmatrix} \,, \quad \lambda^8 = \frac{1}{\sqrt{3}} \begin{pmatrix} 1 & 0 & 0 \\ 0 & 1 & 0 \\ 0 & 0 & -2 \end{pmatrix} \,, \end{aligned} \tag{A.13}$$

which fulfill the relation $\mathrm{Tr}\left[\dfrac{\lambda^i \lambda^j}{4}\right] = \dfrac{1}{2}\delta^{ij}$ and have vanishing trace $\mathrm{Tr}\left[\lambda^i\right] = 0$ [16].

A.4 Wick Rotation

In order to change integration variables from Minkowski to Euclidean space, we use the following convention for a Wick rotation

$$\begin{aligned} k^0 &\longrightarrow i k^0_{\mathrm{E}} \,, \\ k^i &\longrightarrow k^i_{\mathrm{E}} \,, \qquad i = 1, 2, 3 \,, \end{aligned} \tag{A.14}$$

where the index E labels momenta in Euclidean space. Thus, the integration measure changes as $d^4k \longrightarrow i d^4 k_{\mathrm{E}}$ and $k^2 \longrightarrow -k^2_{\mathrm{E}}$.

Appendix B

Numerical Integration Methods

In order to solve the Dyson-Schwinger equation for the fermion propagator, it is necessary to determine the occurring integrals numerically.
The chosen method within this thesis is the Gaussian quadrature rule [56]. It refers to a tool of numerical analysis to calculate the definite integral over the function $f(x)$ on the interval $[-1, 1]$.
Within this numerical approach, the function $f(x)$ is first of all approximated by a weighting function $W(x)$ times a polinomial approximable function $g(x)$.
The integral can then be estimated by a weighted sum of function values at specific points

$$\int_{-1}^{1} f(x)dx = \int_{-1}^{1} W(x)g(x)dx \simeq \sum_{i=1}^{N} w_i g(x_i)\,, \tag{B.1}$$

where x_i with $i = 1, ..., N$ are the N evaluation points, called nodes, and w_i are the according weights.
In the case of f being a polynomial of degree $2N - 1$ or less, Eq. (B.1) is exact.

The calculation of the quadrature nodes and weights depend on the weighting function $W(x)$.
In this thesis we use the common weighting functions $W(x) = 1$ (Gauss-Legendre Quadrature) and $W(x) = \sqrt{1 - x^2}$ (Chebyshev-Gauss Quadrature).

B.1 Gauss- Legendre Quadrature

In the case of $W(x) = 1$, the N nodes x_i are given by the roots of the N-th Legendre Polynomial $P_N(x)$and the according weights are [56]

$$w_i = \frac{2}{\left(1 - x_i^2\right)\left(P_N'(x_i)\right)^2}\,. \tag{B.2}$$

The N-th Legendre Polynomial is defined recursively by

$$\begin{aligned} P_0(x) &= 1\,, \\ P_1(x) &= x\,, \\ (N+1)P_{N+1}(x) &= (2N+1)xP_N(x) + NP_{N-1}(x)\,, \qquad . \end{aligned} \tag{B.3}$$

For a Gauss-Legendre quadrature on a logarithmic scale over a general finite interval $[a, b]$ we first have to substitute the integration variable $e^y = t$ and afterwards change the bounds of integration to $[-1, 1]$ by a second substitution $y = \frac{1}{2}\ln\left(\frac{b}{a}\right)x + \frac{1}{2}\ln(ab)$.
This yields finally:

$$\begin{aligned} \int_a^b f(t)dt &= \int_{\ln a}^{\ln b} f(e^y)e^y dy\,, \qquad\qquad y = \ln(t) \\ &= \frac{1}{2}\ln\left(\frac{b}{a}\right)\int_{-1}^{1} f\left(\exp\left[\frac{1}{2}\ln\left(\frac{b}{a}\right)x + \frac{1}{2}\ln(ab)\right]\right)\exp\left[\frac{1}{2}\ln\left(\frac{b}{a}\right)x + \frac{1}{2}\ln(ab)\right]dx \\ &\approx \frac{1}{2}\ln\left(\frac{b}{a}\right)\sum_{i=1}^{N} w_i f\left(\exp\left[\frac{1}{2}\ln\left(\frac{b}{a}\right)x_i + \frac{1}{2}\ln(ab)\right]\right)\exp\left[\frac{1}{2}\ln\left(\frac{b}{a}\right)x_i + \frac{1}{2}\ln(ab)\right]. \end{aligned} \tag{B.4}$$

B.2 Chebyshev-Gauss Quadrature

For the angular part of the considered integrals, the weighting function in Eq. (B.1) is given by $W(x) = \sqrt{1-x^2}$.
In this case, the Chebyshev-Gauss Quadrature is applied where the nodes and weights take the simple form [57]

$$\begin{aligned} x_i &= \cos\left(\frac{i}{N+1}\pi\right), \\ w_i &= \frac{\pi}{N+1}\sin^2\left(\frac{i}{N+1}\pi\right), \qquad\qquad i = 1, ..., N\,. \end{aligned} \tag{B.5}$$

Thus, the complete integral is estimated by

$$\int_{-1}^{1} f(x)dx = \int_{-1}^{1}\sqrt{1-x^2}\,g(x)dx \simeq \sum_{i=1}^{N} w_i g(x_i)\,. \tag{B.6}$$

Acknowledgements

First of all, I would like to thank my supervisor Prof. Dr. Dr. h.c. Manfred Lindner, for giving me the opportunity to write my master thesis at the Max-Planck Institut für Kernphysik and to learn from his great expertise.
Furthermore, I would like to thank Prof. Dr. Joerg Jaeckel for agreeing to become my second referee.

My special thanks goes to Dr. Andreas Trautner for the many fruitful discussions, plenty of good advice and motivating words, always being available and answering my questions. My sincere thanks also goes to Dr. Thomas Hugle, Christian Doering and Daniel Winkler for proofreading my thesis.

Also I wish to thank Marcel Neugebauer for his unfailing emotional support and care within the last months and for his overall companionship that enriched my master studies from the very first day.

Last but not least, none of this could have happened without my family. I would especially like to thank my parents Dr. Regine Peschina-Klett and Dr. Alfred Klett for their never ending love and encouragement. Their advice is dear and precious to me and provides support in every condition of life. Furthermore, I like to thank Lara Klett who is a perfect big sister, best friend and great flatmate at once helping and cheering me forever and ever.

Bibliography

[1] S.L. Glashow. Partial Symmetries of Weak Interactions. *Nucl.Phys.*, 22:579–588, 1961.

[2] S. Weinberg. A Model of Leptons. *Phys. Rev. Lett.*, 19(1264), 1967.

[3] A. Salam. Weak and Electromagnetic Interactions. *Conf.Proc.C*, (680519):367–377, 1968.

[4] D. J. Gross, F. Wilczek. Asymptotically Free Gauge Theories. I. *Phys. Rev. D*, 8(3633), 1973.

[5] D. J. Gross, F. Wilczek. Asymptotically Free Gauge Theories. II. *Phys. Rev. D*, 9(980), 1974.

[6] H.D. Politzer. Asymptotic Freedom: An Approach to Strong Interactions. *Phys.Rept.*, 14:129–180, 1974.

[7] F. Englert and R. Brout. Broken Symmetry and the Mass of Gauge Vector Mesons. *Phys. Rev. Lett.*, 13(321), 1964.

[8] P.W. Higgs. Broken Symmetries and the Masses of Gauge Bosons. *Phys. Rev. Lett.*, 13(508), 1964.

[9] D. Lüst, E. Papantonopoulos, G. Zoupanos. Dynamical Fermion Mass Hierachy and Flavour Mixing. *Z Phys. C*, 25:81–90, 1984.

[10] D. Lüst, E. Papantonopoulos, K.H. Streng, G. Zoupanos. Phenomenology of High Colour Fermions. *Nuc. Phys. B*, 268:49–78, 1986.

[11] R. Alkofer, L. Smekal. The Infrared Behaviour of QCD Green'sFunctions. *Phys.Rept.*, 353:281, 2001. arXiv:hep-ph/0007355v2.

[12] M. E. Peskin, T. Takeuchi. New constraint on a strongly interacting Higgs sector. *Phys. Rev. Lett.*, 65(964), 1990.

[13] M. Tanabashiet al. (Particle Data Group), Revised March 2018 by J. Erler (U. Mexico) and A. Freitas (PittsburghU.). Electroweak model and constraints on new physics. *Phys. Rev. D*, 98(030001):161–179, 2018.

[14] Y. Okada. LHC signatures of vector-like quarks. *Adv.High Energy Phys.*, 2013(364936), 2013.

[15] H. Georgi. *Lie Algebras in Particle Physics. From Isospin to Unified Theories.* Westview Press, 2 edition, 1999.

[16] P. Langacker. *The Standard Model and Beyond.* CRC Press, 2 edition, 2017.

[17] J.F. Cornwell. *Group Theory in Physics. An Introduction.* Academic Press, 1 edition, 1997.

[18] G. Eichmann. Introduction to hadron physics. *Lecture Notes, University of Giessen*, 2014. `http://cftp.ist.utl.pt/~gernot.eichmann/ws2014`, 21.8.2020.

[19] R. Slansky. Group theory for unified model building. *Phys. Rept.*, 79(1):1–128, 1981.

[20] R. Feger, T.W. Kephart, R.J. Saskowski. LieART 2.0. A Mathematica application for Lie Algebras and Representation Theory. *Comput.Phys.Commun.*, 257(107490), 2020.

[21] A. Love D. Bailin. *Introduction to Gauge Field Theory.* Taylor and Francis Group, 1993.

[22] L.D. Faddeev, V.N. Popov. Feynman diagrams for the Yang-Mills field. *Phys. Rev. B*, 25(1):29–30, 1967.

[23] C. Becchi, A. Rouet, R. Stora. Renormalization of gauge theories. *Annals Phys.*, 98(2):287–321, 1976.

[24] M. Z. Iofa, I. V. Tyutin. Gauge invariance of spontaneously broken non-Abelian theories in the Bogolyubov-Parasyuk-Hepp-Zimmermann method. *Theor. Math. Phys.*, 27:316–322, 1976.

[25] M.D. Schwartz. *Quantum Field Theory and the Standard Model.* Cambridge University Press, 1 edition, 2014.

[26] D.V. Schroeder M.E. Peskin. *An Introduction to Quantum Field Theory.* Westview Press, Student Economy Edition, 1995.

[27] M. Tanabashiet al. (Particle Data Group). Quantum Chromodynamics. *Phys. Rev. D*, 98(030001):141–160, 2018.

[28] G. 't Hooft. Computation of the quantum effects due to a four-dimensional pseudoparticle. *Phys. Rev. D*, 14(3432), 1976.

[29] F. J. Yndurain. *The Theory of Quark and Gluon Interactions.* Springer Verlag, 2 edition, 1983.

[30] Edited by T. Ferbel. *Techniques and concepts of High-Energy Physics VIII, NATO ASI Series B: Physics Vol.351.* Springer Science + Business Media New York, originally published by Plenum Press, 1 edition, 1995.

[31] S. Raby, S. Dimopoulos, L. Susskind. Tumbling Gauge Theories. *Nuclear Physics*, B169:373–383, 1980.

[32] V.A. Miransky. *Dynamical Symmetry Breaking in Quantum Field Theories*. World Scientific, 2 edition, 1993.

[33] J. Cornwall, R. Jackiw, E. Tomboulis. Effective Action for composite Operators. *Phys. Rev. D*, 10(8):2428, 1973.

[34] B. Haeri, Jr. Vertices and the CJT effective Potential. *Phys. Rev. D*, 48(12):5930–5934, 1993. arXiv:hep-ph/9309224.

[35] G.'t Hooft, M.Veltman. Regularization and renormalization of gauge fields. *Nuc. Phys. B*, 44(1):189, 1972.

[36] J.C.Taylor. Ward identities and charge renormalization of the Yang-Mills field. *Nuc. Phys. B*, 33(2):436–444, 1971.

[37] H. Zheng. A renormalization group analysis of the Higgs boson with heavy fermions and compositeness. *Phys. Rev. B*, 378:201–206, 1996.

[38] K. Lane. Asymptotic Freedom and Goldstone realization of Chiral Symmetry. *Phys. Rev. D*, 10(8):2605, 1974.

[39] F. J. Yndurain. *Quantum Chromodynamics - An Introduction to the Theory of Quarks and Gluons*. Springer Verlag, 1 edition, 1983.

[40] K. G. Wilson. Non-Lagrangian Models of Current Algebra. *Phys. Rev.*, 179(5):1499, 1969.

[41] H. D. Politzer. Effective Quark Masses in the Chiral Limit. *Nuc. Phys. B*, 117:397–406, 1976.

[42] C. D. Roberts, A. G. Williams. Dyson-Schwinger Equations and their Application to Hadronic Physics. *Prog. Part. Nucl. Phys.*, 33:477–575, 1994. arxiv:hep-ph/9403224.

[43] J. S.Ball, T.-W. Chiu. Analytic properties of the vertex function in gauge theories. *Phys. Rev. D*, 22(10), 1980.

[44] D. C. Curtis, M. R. Pennington. Truncating the Schwinger-Dyson equations: How multiplicative renormalizability and the Ward identity restrict the three-point vertex in QED. *Phys. Rev. D*, 42(12):4165, 1990.

[45] C.D. Roberts, S.M. Schmidt. Dyson-Schwinger equations: Density, temperature and continuum strong QCD. *Prog. Part. and Nuc. Phys.*, 45:S1–S103, 2000. Suplement 1.

[46] P. Isserstedt. Dyson–schwinger approach to the taylor coefficients of the quark pressure, Februaray 2017. `https://theorie.ikp.physik.tu-darmstadt.de/nhq/downloads/thesis/master.isserstedt.pdf`, 17.9.2020.

[47] A. Bender, W. Detmold, A. W. Thomas, C. D. Roberts. Bethe-Salpeter equation and a nonperturbative quark-gluon vertex. *Phys. Rev. C*, 65(65203), 2002.

[48] P. Maris, C. D. Roberts and P. C. Tandy. Pion mass and decay constant. *Phys. Lett.*, B420(267), 1998. arxiv:nucl-th/9707003.

[49] E. Stein W. Greiner, S. Schramm. *Quantum Chromodynamics*. Springer, 2 edition, 2002.

[50] P. Maris and C. D. Roberts. Pi- and K-meson Bethe-Salpeter amplitudes. *Phys. Rev. C*, 56(3369), 1997.

[51] A. Bazavov et al. The chiral and deconfinement aspects of the QCD transition. *Phys. Rev. D*, 85(054503), 2012.

[52] R. Williams, C.S. Fischer, M.R. Pennington. $\overline{q}q$ condensate for light quarks beyond the chiral limit. *Phys. Lett. B*, 645(2-3):167–172, 2007. arxiv:nucl-th/9707003.

[53] R. Williams. *Schwinger–Dyson Equations In QED and QCD - The Calculation of Fermion–Antifermion Condensates*. PhD thesis, Institute for Particle Physics PhenomenologyUniversity of Durham, June 2007. `https://www.ippp.dur.ac.uk/old/export/sites/IPPP/Research/Theses/rwilliams.pdf`, 4.5.2020.

[54] M. Cheng et al. QCD equation of state with almost physical quark masses. *Phys. Rev. D*, 77(014511), 2008.

[55] C. S. Fischer, J. Luecker. Propagators and phase structure of and QCD. *Phys. Lett. B*, 718(1036), 2012.

[56] T. Arens et al. *Mathematik*. Springer Spektrum, 3 edition, 2015.

[57] G. Opfer. *Numerische Mathematik für Anfänger*. Vieweg Teubner, 5 edition, 2008.

Erklärung:

Ich versichere, dass ich diese Arbeit selbstständig verfasst und keine anderen als die angegebenen Quellen und Hilfsmittel benutzt habe.

Heidelberg, den 2.November 2020